Probing the role of Valine 185 of the D1 protein in the Photosystem II oxygen evolution

Miwa Sugiura[a,d], Tania Tibiletti[b,c], Itsuki Takachi[d], Yuya Hara[d], Shin Kanawaku[d], Julien Sellés[e], Alain Boussac[b,*]

[a] Proteo-Science Research Center, Ehime University, Bunkyo-cho, Matsuyama, Ehime 790-8577, Japan
[b] I²BC, UMR CNRS 9198, CEA Saclay, 91191 Gif-sur-Yvette, France
[c] Société Civile Synchrotron SOLEIL, L'Orme des Merisiers, 91192 Gif-sur-Yvette, France
[d] Graduate School of Science and Technology, Ehime University, Bunkyo-cho, Matsuyama, Ehime 790-8577, Japan
[e] Institut de Biologie Physico-Chimique, UMR CNRS 7141 and Sorbonne Université, 13 rue Pierre et Marie Curie, 75005 Paris, France

ARTICLE INFO

ABSTRACT

In Photosystem II (PSII), the Mn_4CaO_5-cluster of the active site advances through five sequential oxidation states (S_0 to S_4) before water is oxidized and O_2 is generated. The V185 of the D1 protein has been shown to be an important amino acid in PSII function (Dilbeck et al. Biochemistry 52 (2013) 6824–6833). Here, we have studied its role by making a V185T site-directed mutant in the thermophilic cyanobacterium *Thermosynechococcus elongatus*. The properties of the V185T-PSII have been compared to those of the WT*3-PSII by using EPR spectroscopy, polarography, thermoluminescence and time-resolved UV–visible absorption spectroscopy. It is shown that the V185 and the chloride binding site very likely interact *via* the H-bond network linking Tyr_Z and the halide. The V185 contributes to the stabilization of S_2 into the low spin (LS), $S = 1/2$, configuration. Indeed, in the V185T mutant a high proportion of S_2 exhibits a high spin (HS), $S = 5/2$, configuration. By using bromocresol purple as a dye, a proton release was detected in the $S_1Tyr_Z \cdot \rightarrow S_2{}^{HS}Tyr_Z$ transition in the V185T mutant in contrast to the WT*3-PSII in which there is no proton release in this transition. Instead, in WT*3-PSII, a proton release kinetically much faster than the $S_2{}^{LS}Tyr_Z \cdot \rightarrow S_3Tyr_Z$ transition was observed and we propose that it occurs in the $S_2{}^{LS}Tyr_Z \cdot \rightarrow S_2{}^{HS}Tyr_Z \cdot$ intermediate step before the $S_2{}^{HS}Tyr_Z \cdot \rightarrow S_3Tyr_Z$ transition occurs. The dramatic slowdown of the $S_3Tyr_Z \cdot \rightarrow S_0Tyr_Z$ transition in the V185T mutant does not originate from a structural modification of the Mn_4CaO_5 cluster since the spin $S = 3$ S_3 EPR signal is not modified in the mutant. More probably, it is indicative of the strong implication of V185 in the tuning of an efficient relaxation processes of the H-bond network and/or of the protein.

1. Introduction

Photosystem II (PSII) is the light-driven water-splitting enzyme in cyanobacteria, alga, and plants. Water splitting activity results in oxygen evolution and only PSII is able to provide dioxygen into the earth that is essential for aerobic organisms. In cyanobacteria, the PSII complex comprises 17 trans-membrane and 3 extrinsic membrane proteins [1]. X-ray crystal structure revealed the cofactors and metal ions that are 35 chlorophylls *a*, 2 pheophytins (Phe), 2 hemes, 1 non-heme iron, 2 plastoquinones (Q_A and Q_B), the Mn_4CaO_5 cluster, 2 Cl^-, 12 carotenoids and 25 lipids bind to these 20 subunits [1,2]. Most of cofactors relating the water oxidation and electron transfer bind to the

reaction center subunits, D1 and D2.

The first step in the photosynthetic electron transfer chain is the excitation of one of the chlorophylls upon the absorption of a photon by the Chl antennae. Then, the excitation is transferred to the photochemical trap which includes the four chlorophylls; P_{D1}, P_{D2}, Chl_{D1} and Chl_{D2}. A charge separation occurs after a few picoseconds following the light-absorption process forming the $Chl_{D1}^+Phe_{D1}^-$ and then the $P_{D1}^+Phe_{D1}^-$ radical pair states, *e.g.* [3,4] and references therein. P_{D1}^+ then oxidizes Tyr_Z, the Tyr161 of the D1 polypeptide, which in turn oxidizes the Mn_4CaO_5 cluster, *e.g.* [2,5–8] for reviews. The electron on Phe_{D1}^- is then transferred to Q_A, the primary quinone electron acceptor and then to Q_B, the second quinone electron acceptor. Whereas Q_A can be only singly reduced under normal conditions, Q_B accepts two electrons and two protons before to leave its binding site, *e.g.* [9–11] and references therein.

The Mn_4CaO_5 cluster is sequentially oxidized following each charge separation so that it cycles through five redox states denoted S_n, where n stands for the number of stored oxidizing equivalents [12,13]. When the S_4-state is formed, *i.e.* after the 3rd flash of light given on dark-adapted PSII, the two water molecules bound to the cluster are oxidized, the O_2 is released and the S_0-state is reformed.

The dark-stable S_n-state is the S_1-state. The S_1-state to S_2-state transition can be induced either by a single flash illumination given at room temperature or by a continuous illumination given between 140 K and 230 K. Indeed, in this temperature interval, the S_1-state may progress to the S_2-state while the electron transfer from Q_A^- to Q_B cannot thus preventing a second oxidation of the Mn_4CaO_5 cluster [9,10].

EPR measurements performed at helium temperatures show that the S_2-state may have either a low spin $S = 1/2$ configuration or a high spin $S_G = 5/2$ configuration, reviewed in Ref. [14,15]. The $S = 1/2$ configuration, S_2^{LS}, exhibits a multiline signal centered at $g \approx 2.0$ which spreads over ≈ 1800 gauss. This multiline signal is made up of at least 20 lines, separated by approximately 80 gauss [16]. The $S_G = 5/2$ configuration, S_2^{HS}, exhibits a derivative-like EPR signal centered at $g \approx 4.1$ [17,18]. Other more complex signals may be observed at lower magnetic fields (*i.e.* at higher g values) which are attributed to high spin states with $S \geq 5/2$ [19,20]. The S_2^{LS}-state contains one Mn^{III} ion and three Mn^{IV} ions from ENDOR and X-ray spectroscopies [21,22]. In the S_2^{LS} configuration the net oxidation state of the 4 Mn ions is considered to be: $Mn4^{IV}$, $Mn3^{IV}$, $Mn2^{IV}$, $Mn1^{III}$. In this structure, the Mn4 and Mn3 are connected by a di-μ-oxo bridge, with O4 and O5 the bridging oxygen, while the Mn1, Mn2, Mn3, Ca and O1, O2 and O3 are the vertex of an open cubane structure in which there is no connection between O5 and Mn1.

From the crystal structure of PSII in the S_1-state [1,2], it has been suggested from *in silico* studies [23] that the S_2^{LS}-state and S_2^{HS}-state had almost isoenergetic structures sharing the same coordination environment with the Mn^{III} ion located on Mn1 in the S_2^{LS}-state and on the Mn4 in the S_2^{HS}-state. This valence swap between the Mn1 and Mn4 was further proposed [23–25] to be associated with a structural change in which the oxygen O5 linking the Mn4, Mn3 and the Ca in the S_2^{LS} configuration moved to a position closing the cubane by bridging the Mn1, Mn3 and Ca ions. It has been recently shown that the equilibrium between S_2^{LS} and S_2^{HS} is pH dependent [26], with a $pK_a \approx 8.3$ for the native Mn_4CaO_5 and $pK_a \approx 7.5$ for Mn_4SrO_5. DFT results suggested that exchanging Ca with Sr modifies the electronic structure of several titratable groups within the active site, including groups that are *not* direct ligands to Ca/Sr, *e.g.* W1/W2, D61, H332 and H337, consistently with the complex modification of the pK_a upon the Ca/Sr exchange [26].

The S_1-state progresses to the S_3-state by giving 2 flashes at room temperature. The full X-band EPR spectrum [27] of the S_3-state was simulated assuming a spin $S_G = 3$ [27,28]. It was further proposed from a multi-frequency, multi-dimensional magnetic resonance spectroscopy that all four Mn ions are structurally and electronically similar with a + 4 formal oxidation state in an octahedral ligation sphere with the

cluster in an open cubane configuration [29]. In both Ca-PSII and Sr-PSII, the S_2^{HS} state was found capable of advancing to S_3 at low temperature (198 K) [26,30]. This was taken as an experimental demonstration that the S_2^{LS} is formed first and advances to S_3 *via* the S_2^{HS}-state without detectable intermediates in agreement with earlier works in plant PSII [31]. Several experimental and computational studies, listed in Ref. [26], suggest the existence of more than one structural form of S_3: 1) the dominant S_3 exhibiting the $S_G = 3$ EPR signal [27–29], and 2) a state that does not give an EPR signal *per se* but which is manifest as an EPR signal generated by near-IR illumination (between 760 and 820 nm) at low temperature [32] in approximately 30 to 40% of the centers [33].

The current view is that in the S_n-state cycle, the S_2 state formed from S_1 is the S_2^{LS} state. Then, it has been proposed from *in silico* studies that the formation of $Tyr_Z\cdot$ in the S_2^{LS}-state induces a reorientation of the dipole moment of the Mn_4CaO_5 cluster such that the locus of the negative charge becomes directed towards W1 and its hydrogen bonding partner, D1-D61 [34] resulting in a shift of the equilibrium $S_2^{LS} \leftrightarrow S_2^{HS}$ in favor of the high spin configuration, the only configuration capable to donate an electron to $Tyr_Z\cdot$ in this model. Alternatively, the formation of $Tyr_Z\cdot$ was proposed to affect the pK_a of W3 triggering its movement onto either Mn4 or Mn1 depending on whether the cube is in the closed (HS) or open (LS) configuration [35]. With the HS route being the lower energy option, the route to S_3 *via* the S_2^{HS} intermediate was favored [35]. Although experimental evidences show that the S_2^{LS} is formed first and progresses to S_3 *via* the S_2^{HS}-state without detectable intermediates [26], other mechanisms suggesting that the S_2-state progresses to S_3 from its open cube configuration are also proposed [36–38].

The proton movements occurring during the S_n-state cycle are strongly influenced both by the hydrogen (H)-bonding network involving the first coordination sphere of the Mn_4CaO_5 cluster, and also by the H-bonding network that extends well outside the first coordination sphere, *e.g.* [39–44]. In particular, as mentioned above, biochemical conditions that affect this H-bonding network also modify the S_2-state equilibrium between the S_2^{LS}- and S_2^{HS}-states of the Mn_4CaO_5 cluster. It has been suggested that hydrogen bondings involving W1 and W2, the terminal water molecules bound to Mn4, could play and important role in this equilibrium, *e.g.* [45].

With the aim to identify which amino acids outside the first coordination sphere of the Mn_4CaO_5 are involved in a network tuning the properties of the cluster, a great number of site-directed mutants have been constructed and studied. Among the residues studied and belonging either to D1 or D2, there are the D1-E65, D2-E312 and D1-E329 [46], the D1-D61 [47], the D1-R334, D1-Q165, D2-D307, D2-E308, D2-D310 and D2-D323 [48], the D1-N181 [49], the D1-N298 [50], the D1-N87 [51], the D1-I60, D1-G166 and D1-S169 [52], the D1-P173 [53], and the D1-V185 [52,54]. The mutation of the hydrophobic D1-V185 [44,52,54] which is in the vicinity of water molecules located between Tyr_Z and D1-D61 (Fig. 1), was done in *Synechocystis* sp. PCC 6803 (hereafter *Synechocystis* 6803) with the aim to perturb a region including water molecules interacting with the Mn_4CaO_5 cluster, the ligands of the Mn_4CaO_5 cluster, Tyr_Z, and the chloride binding site [52,54]. The most perturbed active mutant was D1-V185N in which the O_2 evolution rate was significantly diminished with a higher miss factor than that for the wild type. This substitution dramatically slowed down the two steps $S_3Tyr_Z\cdot \rightarrow (S_3Tyr_Z\cdot)' \rightarrow S_0Tyr_Z + O_2$. As mentioned by the authors [52], a similar slowing down was observed in the D1-D61N mutant [55]. In a recent FTIR study [44], it has been shown that the V185N mutant in *Synechocystis* 6803 had the most perturbed H-bond network of all the mutants studied until now and that, without directly affecting the water molecules interacting with D1-D61.

To decipher the consequences of these extensive modifications in the H-bond network, a D1-V185T mutant has been constructed in the thermophilic cyanobacterium *Thermosynechococcus elongatus* (hereafter *T. elongatus*). The replacement of V185 by T in *Synechocystis* 6803 was
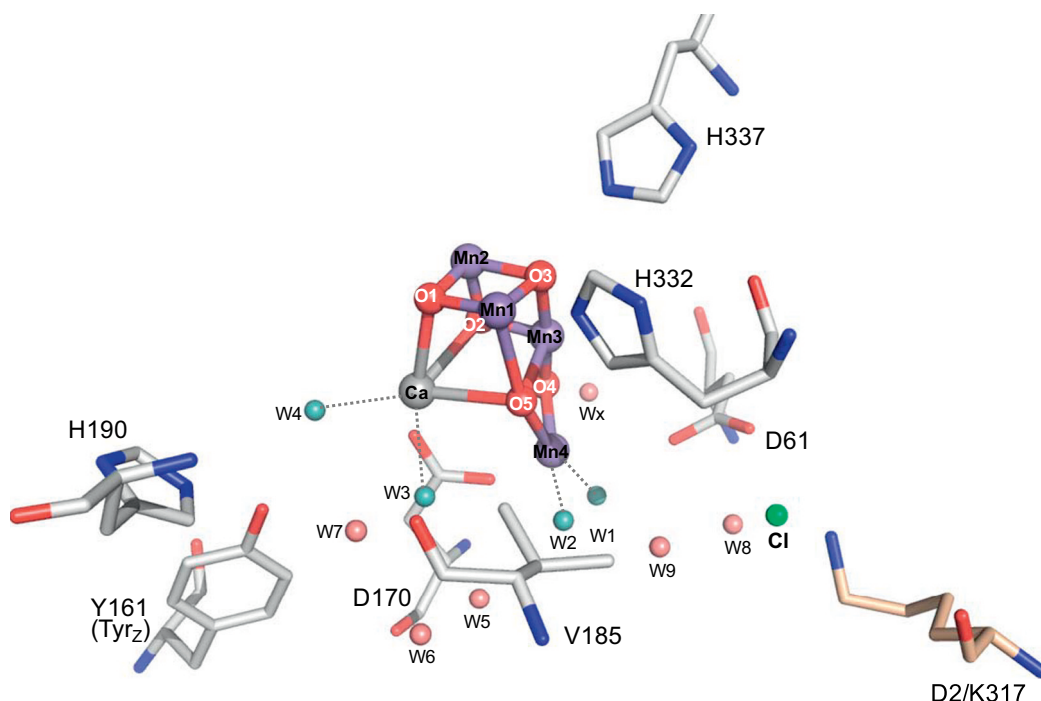
Fig. 1. Structure of the Mn_4CaO_5 cluster and the surrounding environment [1]. Water molecules (W1–W4) drawn in blue are ligands of the cluster. Other water molecules (W5-W9 and Wx) in pale red are molecules hydrogen bonded to amino acid residues around the cluster. The D61, Y161, V185, H332 and H337 are amino acids of the D1 polypeptide. The figure was drawn with Mac-PyMOL with the A monomer in PDB 4UB6.

not the most disrupting mutation [52] but, as shown here, in *T. elongatus* it induced important modifications in the function of the enzyme. In this work, we characterized the mutant D1-V185T in *T. elongatus* by a combination of techniques like O_2 polarography by using either a Clark-type electrode under continuous illumination or a rate electrode under illumination by flash, EPR spectroscopy, thermoluminescence, UV–visible time-resolved absorption changes spectroscopy including proton release detection under flash illumination.

2. Materials and methods

2.1. Construction of the V185T mutant and Photosystem II preparation

The *T. elongatus* strain used was the $\Delta psbA_1$, $\Delta psbA_2$ deletion mutant, called WT*3 [56], constructed from the *T. elongatus* 43-H strain that had a His_6-tag on the carboxy terminus of CP43 [57]. For the construction of the V185T site-directed mutant, the positions at +552, +553 and +554 in $psbA_3$ were substituted on a plasmid DNA in order to introduce a V185T substitution and to create a restriction site of *Acl* I by a Quick–Change Lightning Site–Directed Mutagenesis Kit (Agilent Technologies) as shown in Fig. 2A [56]. After introduction of the plasmid DNA into the host cells by using an electroporator (BioRad gene pulser), mutant cells were selected from the cells on DTN agar plate containing $5 \mu g \, mL^{-1}$ of chloramphenicol (Cm), $25 \mu g \, mL^{-1}$ of spectinomycin, $10 \mu g \, mL^{-1}$ of streptomycin, and $40 \mu g \, mL^{-1}$ of kanamycin as previously described [56]. Fig. 2C shows results of the genomic DNA analyses around site-directed mutation of segregated cells. After PCR amplification of the mutated region by using a forward primer (Fw; 5′–CTACAACGGTGGCCCCTACCAACTG–3′) and a reverse primer (Rv; 5′–GCTGATACCCAGGGCAGTAAACCAGATGCC–3′) (Fig. 2B), the PCR products were digested with *Acl* I. As shown in Fig. 2C, amplified 554-bp DNA fragments (Fig. 2C, lane 4) were completely digested with *Acl* I in V185 mutant genome (lane 5). In contrast to V185T genome, the amplified 554-bp DNA fragments in WT*3 genome could not be digested with *Acl* I (lanes 2 and 3). To make sure, the genomic DNA sequence of the open reading frame of $psbA_3$ was confirmed by nucleotides sequencing by using a GenomeLab GeXP DNA sequencer (Beckman Coulter).

The biosynthetic Ca/Sr and Cl/Br exchanges and PSII purifications were achieved as previously described [53,58]. Native PSII is designated Ca-PSII. PSII in which Sr^{2+} was substituted for Ca^{2+} is designated Sr-PSII. PSII in which Br^- was substituted for Cl^- is designated Br-PSII. The purified Ca-PSII and Sr-PSII were suspended in 1 M betaine, 15 mM $CaCl_2$, 15 mM $MgCl_2$, 40 mM MES, pH 6.5 (or 15 mM $CaBr_2$ and 15 mM $MgBr_2$ for Br-PSII), then frozen in liquid nitrogen until use.

2.2. SDS-polyacrylamide gel electrophoresis

Purified PSII (8 μg Chl each) suspended in 40 mM MES/NaOH (pH 6.5), 10 mM NaCl, 10 mM $CaCl_2$, 10 mM $MgCl_2$, 0.03% *n*-dodecyl-β-ᴅ-maltoside were solubilized with 2% lithium laurylsulfate, and then analyzed by an SDS-polyacrylamide 16–22% gradient gel electrophoresis containing 7.5 M urea as previously described [59].

2.3. Oxygen evolution

Oxygen evolution under continuous illumination was measured at 25°C by polarography using a Clark type oxygen electrode (Hansatech) with saturating white light through infrared and water filters. The initial activity was measured in the presence of 0.5 mM 2,6-dichloro-*p*-benzoquinone (DCBQ), dissolved in DMSO, as an electron acceptor. The medium used contained 20 mM Good's buffer and 15 mM $CaCl_2$ (or $CaBr_2$), 15 mM $MgCl_2$ (or $MgBr_2$) and 20 mM NaCl (or NaBr). MES was used for pH 5.0, 5.5, 6.0, 6.5 and 7.0, HEPES was used for pH 7.5 and 8.0, and CHES was used for pH 8.5.

Oxygen evolution under flashing light was measured with a laboratory-made rate electrode [58]. Typically, 25 μl of a thylakoid suspension at 1 mg of Chl mL^{-1} was deposited onto the platinum electrode. The volume of the circulating medium was ≈250 ml and contained 1 M M betaine, 15 mM $CaCl_2$, 15 mM $MgCl_2$, 50 mM KCl, and 40 mM MES, pH 6.5 (pH adjusted with NaOH). Illumination was done with a xenon flash (PerkinElmer Optoelectronics). The intensity of the flash was adjusted so that the light intensity was saturating (*i.e.* the miss parameter was minimum). Measurements were done at room temperature (20–25°C). The amplified amperometric signal resulting from the flash-induced oxygen evolution was recorded with a numerical oscilloscope.
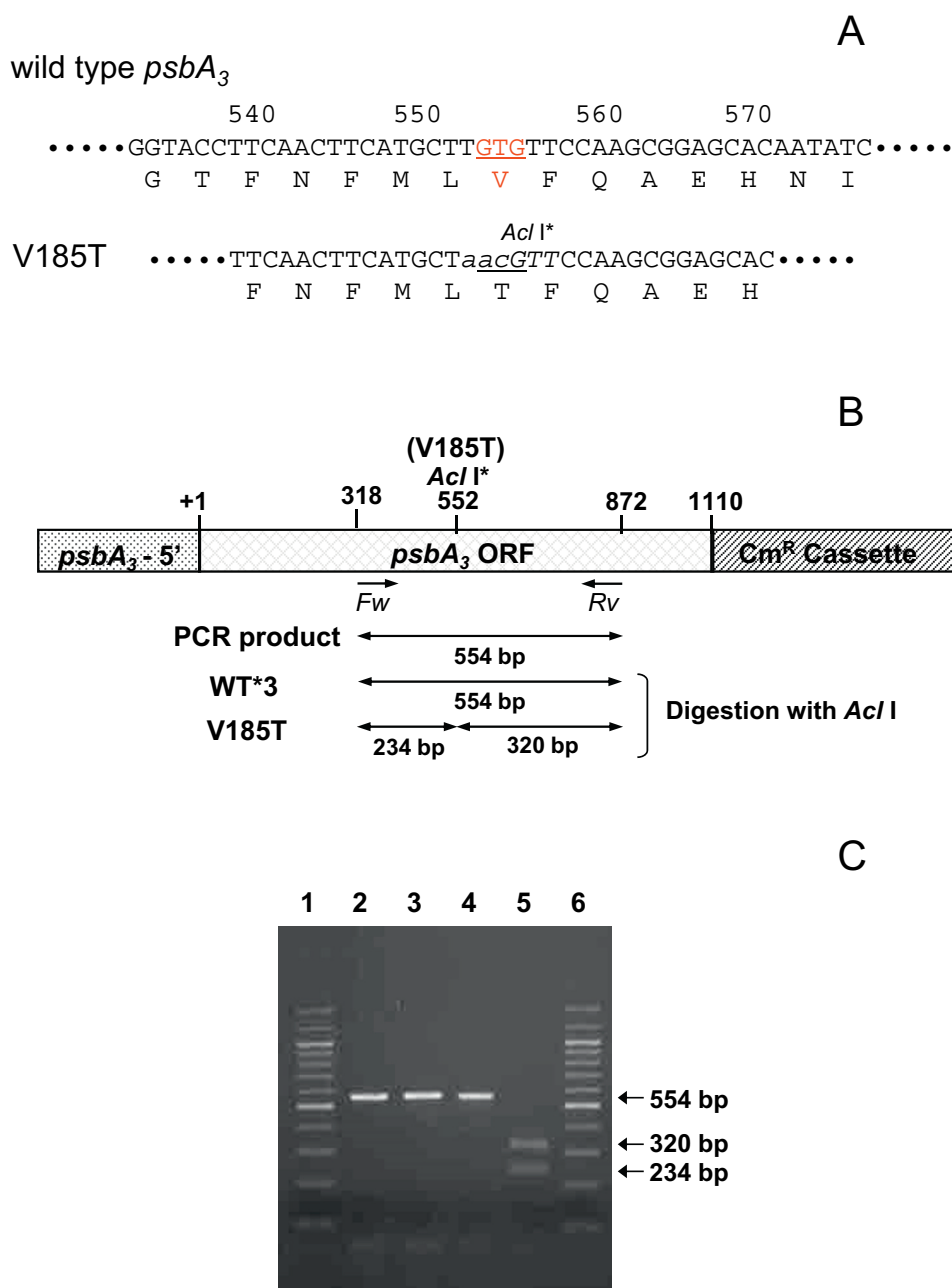
A

wild type *psbA₃*

```
          540         550         560         570
• • • • •GGTACCTTCAACTTCATGCTTGTGTTCCAAGCGGAGCACAATATC• • • • •
         G  T  F  N  F  M  L  V  F  Q  A  E  H  N  I
```

Acl I*

V185T
```
• • • • •TTCAACTTCATGCTaacGTTCCAAGCGGAGCAC• • • • •
         F  N  F  M  L  T  F  Q  A  E  H
```

B

Fig. 2. Construction and confirmation of the *psbA₃* gene in V185T site-directed mutant cells. (A) Nucleotide sequence of *psbA₃* and the amino acid sequences around V185 in the WT*3 strain and the PsbA3-V185T mutant. Positions of V185 is indicated with red letters. Numbers correspond to the position from the initial codon. Substituted nucleotides for V185T in the mutant are indicated in small letters. For making and selection of mutant, the *Acl* I restriction site (letters in italic) was created in *psbA₃*-Thr185 in the same time. (B) Physical map around *psbA₃*, and theoretical length of amplified DNA by PCR using *Forward* (*Fw*) and *Reverse* (*Rv*) primers. The created *Acl* I (shown as *Acl* I*) site for V185T mutant is at position +552. The sizes of 554 bp, 234 bp + 320 bp are DNA fragments after digestion of the amplified DNA with *Acl* I. (C) Agarose gel (2%) electrophoresis of PCR products using the *Fw* and *Rv* primers (lanes 2 and 4) and the DNA fragments of the products after digestion with *Acl* I (lanes 3 and 5). Lane 1 and 6, 100 bp DNA ladder markers (Nacalai, Japan); lanes 2 and 3, WT*3 strain; lanes 4 and 5, V185T strain.

C

2.4. EPR spectroscopy

X-band cw-EPR spectra were recorded with a Bruker Elexsys 500 X-band spectrometer equipped with a standard ER 4102 (Bruker) X-band resonator, a Bruker teslameter, an Oxford Instruments cryostat (ESR 900) and an Oxford ITC504 temperature controller. Flash illumination at room temperature was provided by a neodymium:yttrium–aluminum garnet (Nd:YAG) laser (532 nm, 550 mJ, 8 ns Spectra Physics GCR-230-10). For visible light illumination a 800 W tungsten lamp filtered by water and infrared cut-off filters was used. Illuminations for approximately 5–10 s at temperatures close to 198 K were done in a non-silvered Dewar in ethanol cooled with dry ice.

PSII samples were loaded in the dark into quartz EPR tubes at 1.1 mg of Chl mL^{-1} and dark-adapted for 1 h at room temperature. The samples were then synchronized in the S_1-state with one pre-flash [60]. After a further 1 h dark-adaptation at room temperature the samples were frozen in the dark to 198 K in a dry ice ethanol bath and then transferred to 77 K in liquid N_2. Prior to recording the spectra the samples were degassed at 198 K.

2.5. Thermoluminescence measurements

Thermoluminescence (TL) glow curves were measured with a lab–built apparatus [61,62]. Purified PSII were diluted to 10 μg Chl mL^{-1} in 1 M betaine, 40 mM MES, 15 mM MgCl$_2$, 15 mM CaCl$_2$, pH 6.5 and then dark-adapted for 1 h at room temperature. Flash illumination was done at 0 °C by using a saturating xenon flash. One second after the flash illumination, the samples were heated at the constant heating rate indicated in the legend of the figure and TL emission was detected. It has been checked that, after the dilution, the PSII samples had the same OD at 673 nm.

2.6. UV–visible time-resolved absorption change spectroscopy

Absorption changes measurements were measured with a lab-built spectrophotometer [63] in which the absorption changes are sampled

at discrete times by short analytical flashes. These analytical flashes were provided by an optical parametric oscillator pumped by a frequency tripled Nd:YAG laser, producing monochromatic flashes (355 nm, 1 nm full-width at half-maximum) with a duration of 5 ns. Actinic flashes were provided by a second Nd:YAG laser (532 nm), which pumped an optical parametric oscillator producing monochromatic saturating flashes at 700 nm with the same flash-length. The path-length of the cuvette was 2.5 mm. PSII was used at 25 μg of Chl mL^{-1}.

For the detection at 292 nm, PSII samples were diluted a solution containing 1 M betaine, 15 mM $CaCl_2$, 15 mM $MgCl_2$, and 40 mM MES (pH 6.5). PSII samples were dark-adapted for ≈1 h at room temperature (20–22°C) before the addition of 0.1 mM phenyl p–benzoquinone (PPBQ) dissolved in DMSO.

For proton release/uptake detection, a solution containing 1 M betaine, 15 mM $CaCl_2$, 15 mM $MgCl_2$ and 150 μM Bromocresol purple as indicator dye was used [64]. The pH was adjusted to 6.3, the pK_a of the dye, with NaOH. The solution was prepared several days before the measurements and the pH adjusted three days before the experiments. Such a procedure minimizes the drift in the base line at 575 nm during the experiment. After dark adaptation of the PSII in this medium for 1 h at room temperature, 100 μM PPBQ (in DMSO) and 100 μM potassium ferricyanide were added.

3. Results

The *T. elongatus* V185T mutant cells were able to grow photo-autotrophically as fast as WT*3 cells (*i.e.* with a doubling time close to 16 h, not shown) in the standard DTN medium at pH 7.6 under a low light intensity of ≈50 μE. The oxygen evolution activity of the purified V185 T-PSII measured under continuous illumination was found to be approximately 10% of that in the WT*3-PSII sample, *i.e.* ≈420 *vs.* ≈3800 μmol O_2 (mg Chl)$^{-1}$ h^{-1}. The polypeptide pattern in Fig. 3 shows that this weak activity was not due to the lack of one of the most important PSII subunits. As it will be shown below, although some degradation of the Mn_4CaO_5 complex during the PSII purification cannot be totally ruled out as previously reported [44,52,54] upon the mutation of the V185 most of the effects reported in this study can be interpreted as originating from a strong alteration of the S_n-state cycle in the V185T mutant.

Fig. 4 shows the flash-induced O_2 evolution during a sequence of saturating xenon flashes (spaced 400 ms apart) in WT*3 (Panel A) and V185T (Panel B) thylakoids. The samples were previously dark-adapted for 1 h at room temperature on the polarized electrode before the flash light illumination. This technique requires the use of thylakoids (or cells) rather than isolated PSII because sedimentation of the sample on the bare platinum electrode is required. The oscillations with a period of 4 were well identifiable in the WT*3 sample whereas in the V185T sample after the third flash, the oscillating O_2 evolution appeared damped. This result slightly differs from what was observed with the V185N mutant in *Synechocystis* 6803 in which the oscillation remained more visible [52] suggesting more misses in the V185T T. *elongatus* mutant than in the V185N *Synechocystis* 6803 mutant. Panel C shows the kinetics of O_2 release in the WT*3 and V185T samples. The traces shown in Panel C were arbitrarily scaled to the same maximum amplitude of the amperometric signal. As demonstrated by Lavorel [65], the amperometric signal results from the convolution of the diffusion limited O_2 pulse produced instantaneously in a thin layer at the surface of the platinum electrode with the rate constant, k_{ox}, of the S_3Tyr_Z· to $S_0Tyr_Z + O_2$ reaction. By using the full analysis previously described [58] for kinetics recorded with our electrode, the data in Panel C indicates that in the V185T mutant the $t_{1/2}$ for the O_2 release was, as shown thereafter, close to 20 ms. Panel D shows theoretical amperometric signals calculated as previously computed with O_2 produced in a monolayer at the surface of the electrode [58]. The dashed line corresponds to the theoretical response of our electrode when all O_2 is
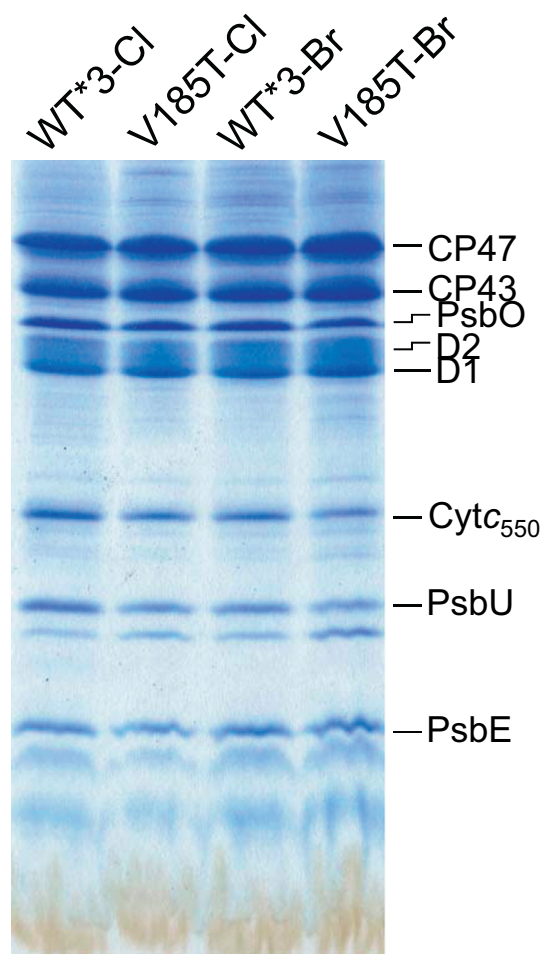

Fig. 3. Coomassie brilliant blue-staining of SDS–polyacrylamide gel electrophoresis of Cl-WT*3-PSII, Br-WT*3-PSII, Cl-V185T-PSII and Br-V185T-PSII. The amount of PSII loaded was 8 μg of Chl for each lane.

produced instantaneously. The trace with a continuous line corresponds to a S_3Tyr_Z· to $S_0Tyr_Z + O_2$ reaction with a $t_{1/2} = 1.5$ ms and the trace with a dotted line corresponds to the same reaction with a $t_{1/2} = 20$ ms. Both for the maximum amplitudes, which appeared approximately 4 times smaller in the mutant (Panel B), and the experimental kinetics are reasonably simulated by using these $t_{1/2}$. The presence of an artefact [52] in the 1 ms time range did not allow us to detect the lag phase in the kinetics reported in Panel C. That will be addressed below.

Fig. 5 shows the amplitude of the absorption changes upon flash illumination recorded in the WT*3-PSII (Panel A) and in the V185 T-PSII (panel B). Measurements were done at 292 nm and in the hundreds of ms time range [66,67], *i.e.* after the reduction of Tyr_Z· by the Mn_4CaO_5 cluster was complete. This wavelength corresponds to an isosbestic point for $PPBQ^-$/PPBQ, the added electron acceptor, and is in a spectral region where the absorption of the Mn_4CaO_5 cluster depends on the S_n-states [67]. The oscillating pattern with a period of four is clearly observed for both samples although in the V185T-PSII they appeared weaker. In WT*3-PSII the miss parameter was ≈9% with ≈100% S_1 in the dark-adapted sample [58]. In the V185T-PSII the miss parameter was calculated to be ≈10% with also almost no S_0Tyr_D· (or S_0Tyr_D/S_1Tyr_D) in the dark-adapted state. Thus, the weaker signal could be due to fewer active centers. To determine which steps could be affected by the mutation in addition to the S_3 to S_0 transition, the absorption changes at 292 nm were measured in the μs to ms time range after each of the first four flashes given to dark-adapted PSII (Fig. 6).

Absorption changes at 292 nm reflect the Mn_4CaO_5 cluster valence changes [67] and the Tyr_Z redox state changes [68] occurring in the
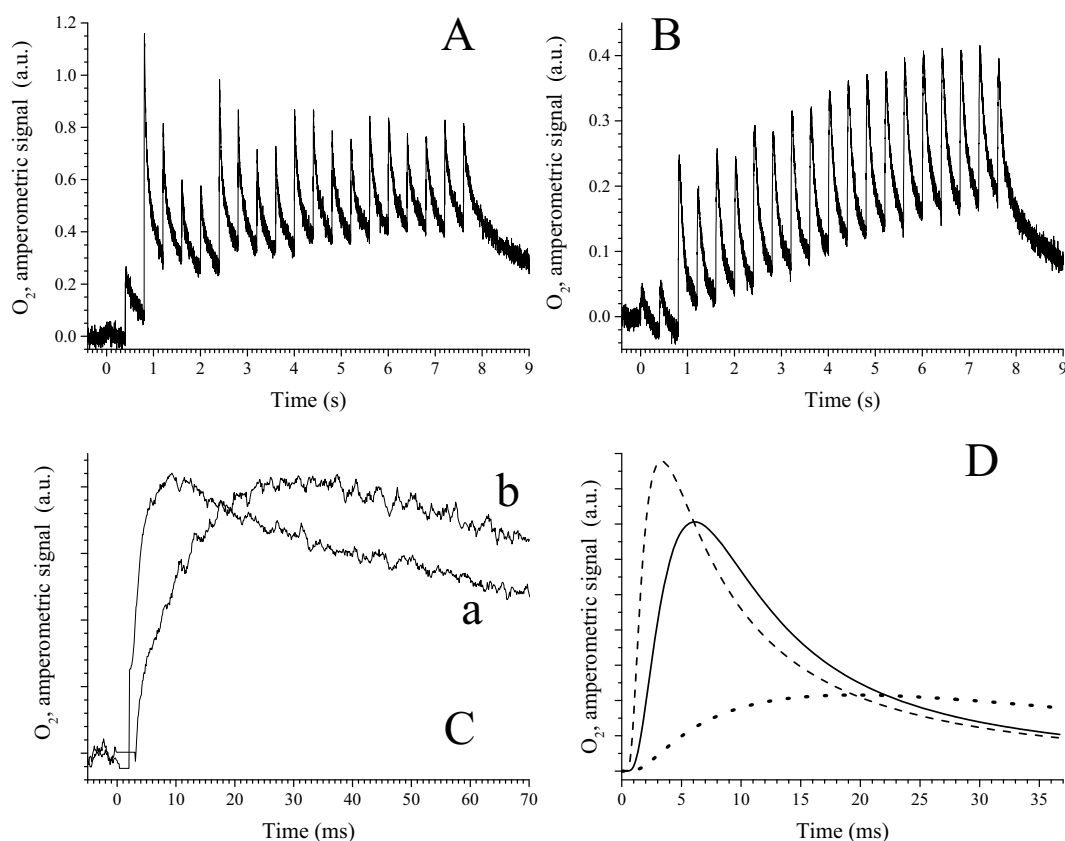
Fig. 4. Flash-induced oxygen evolution on each flash of a sequence of saturating xenon flashes (spaced 400 ms apart) given on WT*3-thylakoids (Panel A) and V185T-thylakoids (Panel B). The samples (Chl ≈ 1 mg/ml) were dark-adapted for 1 h at room temperature on the polarized bare platinum electrode prior to the illumination. Panel C, kinetics of the oxygen release measured after the third flash given on WT*3-thylakoids (trace a) and V185T-thylakoids (trace b) dark-adapted for 1 h on the bare platinum electrode. To normalize the traces, the amplitude of trace b was multiplied approximately four times. Other experimental conditions were as in Panels A and B except that the time scale was sampling time was 10 times faster. Panel D, expected amperometric signal in WT*3-thylakoids (continuous line) and V185T-thylakoids (dotted line). The traces were calculated by using a diffusion time calculated [58]. The dashed line corresponds to the diffusion limited O_2 pulse produced instantaneously in a mono-layer, Φ(t) function, for an experimental diffusion time, t_d, measured equal to 7 ms [58].

$S_1Tyr_Z\cdot \rightarrow S_2Tyr_Z$, $S_2Tyr_Z\cdot \rightarrow S_3Tyr_Z$, $S_3Tyr_Z\cdot \rightarrow S_0Tyr_Z$, and $S_0Tyr_Z\cdot \rightarrow S_1Tyr_Z$ transitions. Only minor absorption changes could be detected after the second flash and the fourth flash. Indeed, the ΔI/I changes associated with the $S_2Tyr_Z\cdot \rightarrow S_3Tyr_Z$ and $S_0Tyr_Z\cdot \rightarrow S_1Tyr_Z$ transitions are small thus precluding the reliable kinetic analysis of the S_2 to S_3 and S_0 to S_1 transitions [67]. On the other hand, because these two transitions only weakly contribute to the absorption changes at this wavelength, the half-times of the $S_1Tyr_Z\cdot \rightarrow S_2Tyr_Z$ and $S_3Tyr_Z\cdot \rightarrow S_0Tyr_Z$

transitions may be reliably determined from the raw data without any deconvolution procedures. The $S_1Tyr_Z\cdot \rightarrow S_2Tyr_Z$ transition was slightly slowed down from $t_{1/2} \approx$ 40–50 μs in WT*3-PSII, Fig. 6A, to $t_{1/2} \approx$ 100–150 μs in V185T-PSII, Fig. 6B. The kinetics of the $S_3Tyr_Z\cdot \rightarrow S_0Tyr_Z$ transition includes a lag phase, *e.g.* [5,58,66] attributed to structural rearrangements in the $S_3Tyr_Z\cdot \rightarrow (S_3Tyr_Z\cdot)'$ in which a proton release occurs. Data in Fig. 6 show that the length of the lag phase was increased from ≈100–200 μs in WT*3-PSII to ≈1–2 ms in
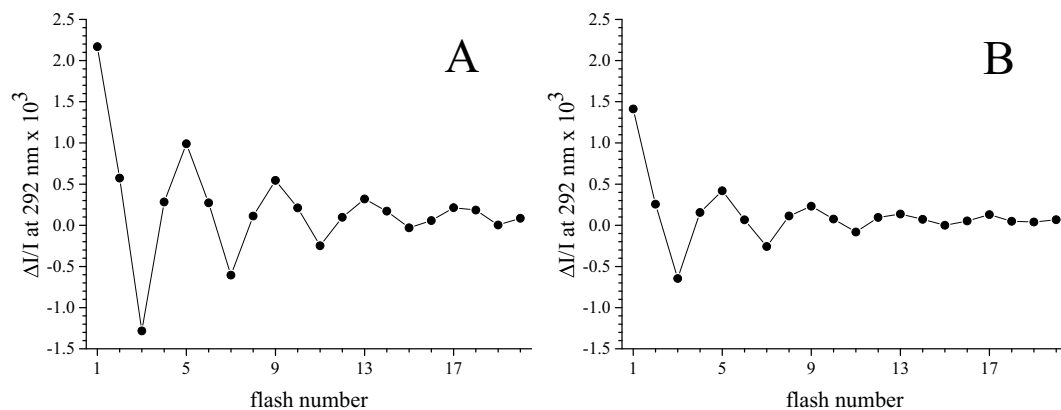

Fig. 5. Sequence of the amplitude of the absorption changes at 292 nm using a series of saturating flashes (spaced 300 ms apart) and given to WT*3-PSII (Panel A) and V185T-PSII (Panel B). The samples (Chl = 25 μg/ml) were dark-adapted for 1 h at room temperature before the addition of 100 μM PPBQ dissolved in dimethylsulfoxyde. The measurements were done 200 ms after each flash.
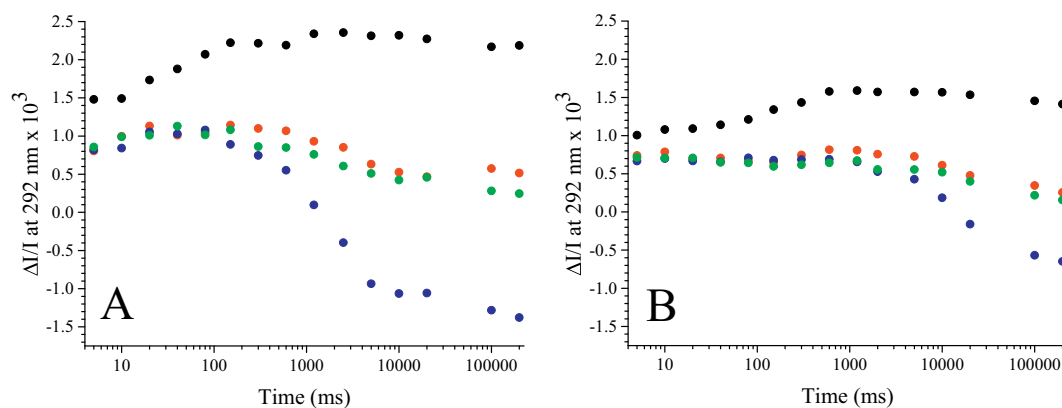
Fig. 6. Kinetics of the absorption changes at 292 nm after the first flash (black points), the second flash (red points), the third flash (blue points), and the fourth flash (green points) given to dark-adapted WT*3-PSII (Panel A) and V185T-PSII (Panel B). Other experimental conditions were similar to those in Fig. 4.

V185T-PSII and that the $(S_3Tyr_Z\cdot)' \rightarrow S_0Tyr_Z$ transition was also dramatically slowed down from $t_{1/2} \approx 1–2$ ms in WT*3-PSII to $t_{1/2} \approx 20$ ms in V185T-PSII. The structural changes induced by the mutation in both the S_2- and S_3-states were further examined by EPR spectroscopy using both Ca-V185T PSII and Sr-V185T PSII. Indeed, we have previously shown that the substitution of Sr for Ca had an effect on the LS/HS ratio in S_2 [26] in WT*3-PSII by involving long-range interactions. For these reasons, the possible effect of the Ca/Sr exchange on this equilibrium in the V185N mutant deserved to be tested.

Formation of the S_2-state was monitored by EPR spectroscopy (Fig. 7) in both Ca-V185T PSII (Panel A) and Sr-V185T PSII (Panel B) after either 1 flash given at room temperature (spectrum a) or continuous illumination for 5 s at 198 K (spectrum b). The spectra shown are the light-*minus*-dark difference spectra. As in previous works [26], no electron acceptor was added to avoid the oxidation of the non-heme iron, which gives an EPR signal that overlaps with parts of the high spin EPR signals in S_2 and with the $S = 3$ S_3 signal. Several observations can be made from these spectra. Firstly, all the light-*minus*-dark difference spectra contained a multiline signal between 2500 and 4200 gauss and signals at magnetic fields below 2200 gauss. These signals at low field are reminiscent, although not identical, of those recorded in samples in which chloride was substituted for iodide [69]. In both Ca-V185T-PSII and Sr-V185T-PSII these low field signals originate from a high spin configuration of the S_2-state. Secondly, the multiline signals in Ca-

V185T-PSII and Sr-V185T-PSII are different and also differ from their counterpart in Ca-WT*3-PSII and Sr-WT*3-PSII [26,30] (see the Supplementary material). Thirdly, whereas the amplitudes of the S_2 multiline signals induced by either 1 flash at room temperature or an illumination at 198 K were similar, the amplitude of the high spin S_2 signals were significantly larger (about twice in Ca-V185T-PSII) after the flash illumination than after the illumination at 198 K. After the 198 K illumination in the Ca-V185T-PSII, there was no evidence for the formation of a Chl^+ or Car^+ radical (see Supplementary material). Instead, some high potential $Cytb_{559}^+$ was induced ($g_z =$ at ≈ 2200 gauss in spectrum b, Panel A) by the illumination at 198 K, but not by the 1 flash illumination, very likely in part of the centers which did not progress to S_2 at 198 K. These data also suggest that the Ca/Sr exchange did not significantly modify the LS/HS equilibrium in the S_2-state of the V185T-PSII. In a small proportion of centers, the 198 K illumination resulted in the formation of a $S_1Tyr_Z\cdot$ split signal seen of the left side of the $Tyr_D\cdot$ signal, something that is more generally observed under illumination at helium temperatures in wild type samples [70,71]. Upon the illumination at 198 K, a large $Q_A^-Fe^{2+}Q_B^-$ signal was induced at $g \approx 1.6$ (turning point at 4200 gauss). This indicates that, in the absence of an added artificial acceptor, Q_B^- was present in a large proportion of centers ($\approx 40\%$) in our dark-adapted *T. elongatus* PSII sample, as previously reported [11].

In Fig. 8, formation of the S_3-state was monitored in the V185T
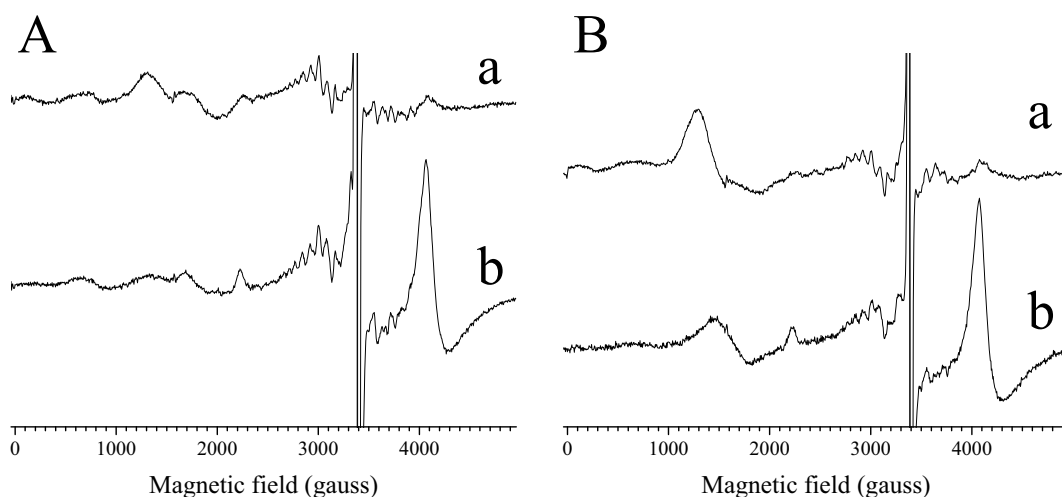
Fig. 7. EPR spectra recorded in Ca-V185T-PSII (Panel A) and Sr-V185T-PSII (Panel B) after either 1 laser flash at room temperature (curves a) or continuous white light illumination at 198 K (curves b). The spectra are the "light"-*minus*-"dark" difference spectra *i.e.* the spectra recorded after illumination *minus* spectra recorded in dark-adapted PSII. [Chl] = 1.1 mg·mL^{-1}. Instrument settings: Temperature, 8.6 K; modulation amplitude, 25 G; microwave power, 20 mW; microwave frequency, 9.4 GHz; modulation frequency, 100 kHz. The saturated signal centered at ≈ 3385 gauss originated from $Tyr_D\cdot$.

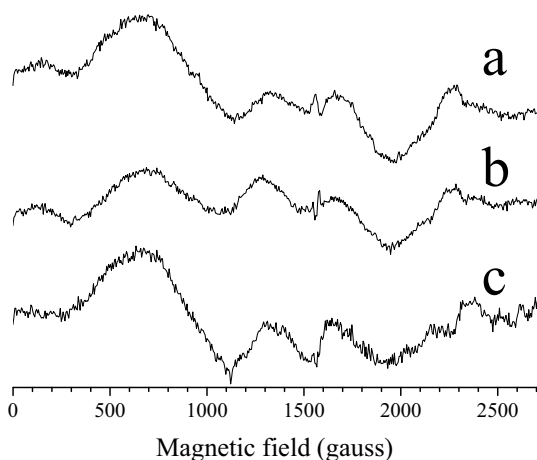**Fig. 8.** EPR spectra recorded in Ca-V185T-PSII (spectrum a), Sr-V185T-PSII (spectrum b) and WT*3-PSII (spectrum c) after 2 laser flashes given at room temperature. The spectra are the "light"-*minus*-"dark" difference spectra *i.e.* the spectra recorded after 2 flashes *minus* spectra recorded in dark-adapted PSII. [Chl] = 1.1 mg·mL^{-1}. Instrument settings: Temperature, 8.6 K; modulation amplitude, 25 G; microwave power, 20 mW; microwave frequency, 9.4 GHz; modulation frequency, 100 kHz.

mutant both in Ca-PSII (spectrum a) and in Sr-PSII (spectrum b). The S$_3$-state was induced by 2 flashes given at room temperature. For comparison, the S$_3$-signal in Ca-WT*3-PSII is also shown (spectrum c). Whereas in S$_2$ the 3 samples exhibited different EPR signals, the S$_3$ signal was affected neither by the V185T mutation nor the Ca/Sr exchange and corresponded to the known $S = 3$ S$_3$ signal [27–29], see also [26] for the similar $S = 3$ S$_3$ EPR signals in Ca-WT*3-PSII and Sr-WT*3-PSII. The amplitude of the $S = 3$ S$_3$ signal was nevertheless slightly smaller in the Sr-V185T-PSII than in the Ca-V185T-PSII.

It has been shown that in both Ca-WT*3-PSII and Sr-WT*3-PSII, the S$_2$^{HS}-state formed from the S$_2$^{LS}-state after increasing the pH was capable of advancing to S$_3$ at low temperature as low as 198 K [26]. This was considered as an experimental demonstration that the S$_2$^{LS} is formed first and advances to S$_3$ *via* the S$_2$^{HS}-state. Fig. 7 shows that both the Ca-V185T-PSII and the Sr-V185T-PSII already exhibited a high proportion of centers in a S$_2$^{HS} configuration at pH 6.5. Therefore, after one flash has previously been given at room temperature to generate S$_2$, a further illumination, without modifying the starting pH value (pH 6.5), was given at 198 K. Fig. 9 Panel A shows the (1 flash + hν 198 K)-*minus*-(1 flash) difference spectra in V185T-Ca-PSII (spectrum a)

and in V185T-Sr-PSII mutant (spectrum b). Panel B is a zoom of the spectra in the low magnetic field region. The 198 K illumination resulted in the formation of the Q$_A$$^-$Fe^{2+}Q$_B$$^-$ signal at $g \approx 1.6$ and in the oxidation of Cytb_{559} in a proportion of centers. More importantly, in both samples, the 198 K illumination induced the loss of the S$_2$^{HS} signal and the appearance of main feature of the $S = 3$ S$_3$ signal centered at ≈ 700 gauss. The 198 K illumination also resulted in the formation of a split signal seen of each side of the Tyr$_D$· signal. In WT*3-PSII, this split signal is similar to that induced in PSII centers in which only the LS configuration is present in S$_2$ and corresponds to the S$_2$^{LS}Tyr$_Z$· split signal [26,71]. Since in the Ca-V185T-PSII the S$_2$^{HS} state is shown to be capable to progress to S$_3$ at 198 K it seems very likely that this split signal also corresponded to the S$_2$^{LS}Tyr$_Z$· state. This split signal appeared smaller in the Sr-V185T-PSII likely because the proportion of S$_2$^{LS} was less in this sample. A possible faster decay of the S$_2$^{LS}Tyr$_Z$·-state in the Sr-V185T-PSII which would originate from a faster tunneling-type back-reaction [72] will be investigated in future studies. It should be noted, mainly in Sr-V185T-PSII, that the S$_2$^{HS} signal that disappeared upon the 198 K illuminations had a different shape that the signal present before the 198 K illumination and induced by 1 flash at room temperature. This likely means that the S$_2$^{HS}-state in the Sr-V185T-PSII is heterogeneous and that only one form is able to perform the S$_2$^{HS} to S$_3$ transition at 198 K. This situation was already met in PSII upon the exchange of chloride for iodide where the high spin form of S$_2$ was unable to advance to S$_3$ at 198 K [69].

In Ca-WT*3-PSII the pH value at which the S$_2$^{LS} configuration fully converts into the S$_2$^{HS} configuration [26] is much higher than the pH value at which the O$_2$ evolution under continuous illumination is the larger, *i.e.* pH ≈ 9.0 *vs.* pH ≈ 6.5 with PPBQ as the added electron acceptor. Panel A in Fig. 10 shows the pH dependency of the O$_2$ evolution under continuous illumination in Cl-WT*3-PSII (black) and Cl-V185T-PSII (red) and Panel B in Fig. 10 shows the O$_2$ evolution in Br-WT*3-PSII (black) and Br-V185T-PSII (red). The effect of the substitution of chloride for bromide was monitored here to have a look for a possible interaction between the V185 residue and the nearby halide. In Ca/Cl-WT*3-PSII, *i.e.* with PsbA3 as D1, the activity was maximum at pH 7.0 as previously observed in Ca/Cl-43H-PSII, *i.e.* with PsbA1 as D1, in the presence of DCBQ [73], the electron acceptor used here. In wild-type PSII, the limiting step under continuous illumination is mainly on the acceptor side which very likely explains the small difference in the pH dependency between PPBQ and DCBQ [73]. In Ca/Cl-V185T-PSII, the optimum pH was down shifted by 1 pH unit to pH 6.0. Upon the Cl/Br exchange, the V185T-PSII and WT*3-PSII samples exhibited an opposite effect with now a similar pH dependence and an optimum at the same pH value, *i.e.* pH = 6.5, in Ca/Br-V185T-PSII and Ca/Br-WT*3-

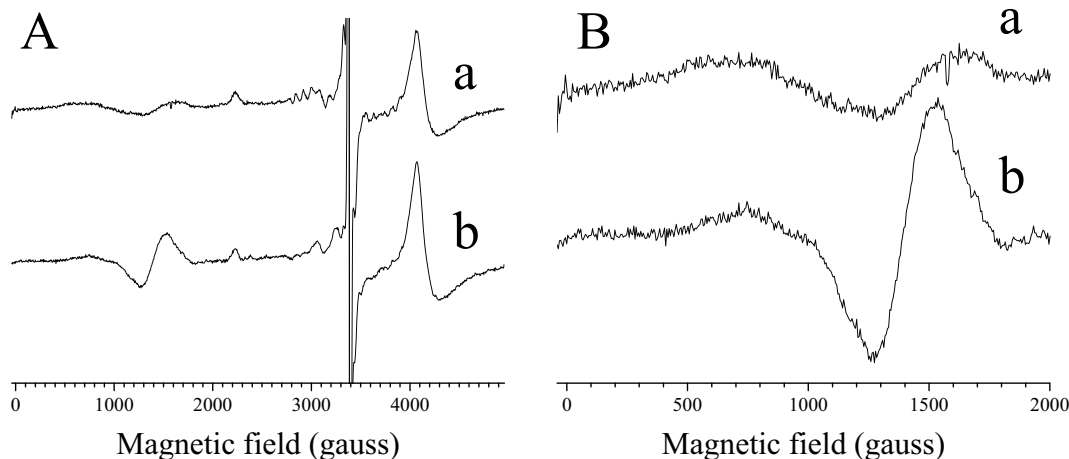**Fig. 9.** Panels A and B: EPR spectra recorded in Ca-V185T-PSII (spectra a) and Sr-V185T-PSII (spectra b) after a continuous white light illumination at 198 K following 1 laser flash given at room temperature. The spectra are difference spectra *i.e.* the spectra recorded after the illumination at 198 K *minus* spectra recorded after 1 flash at room temperature. Same instrument settings as in Fig. 7.
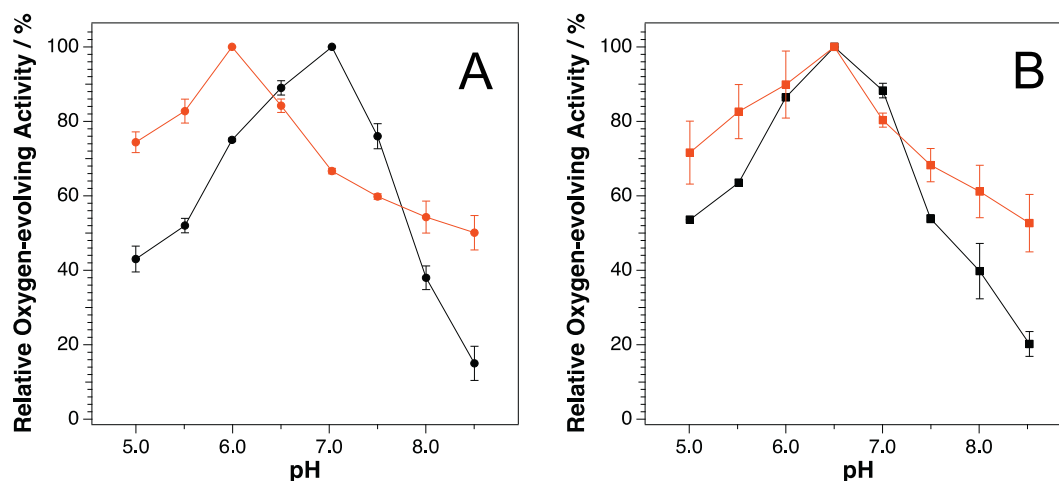
Fig. 10. Relative oxygen-evolving activities at different pH values of Ca/Cl-WT*3-PSII (black) and Ca/Cl-V185T-PSII (red) in Panel A and Ca/Br-WT*3-PSII (black) and Ca/Br-V185T-PSII (red) in Panel B. Absolute values are 3800 μmol O$_2$ (mg Chl)$^{-1}$ h^{-1}, 420 μmol O$_2$ (mg Chl)$^{-1}$ h^{-1}, 1650 μmol O$_2$ (mg Chl)$^{-1}$ h^{-1}, and 370 μmol O$_2$ (mg Chl)$^{-1}$ h^{-1}, in Ca/Cl-WT*3-PSII at pH 7.0, Ca/Cl-V185T-PSII at pH 6.0, Ca/Br-WT*3-PSII at pH 6.5 and Ca/Br-V185T-PSII at pH 6.5, respectively. The values of the activities are the average of at least 3 measurements.

PSII.

During the turnover of the S$_n$-state cycle, the increase in charge resulting from electron abstraction from the Mn$_4$CaO$_5$ cluster is compensated for by proton release(s), thus keeping the redox potential of the catalytic center below that of Tyr$_Z$·/Tyr$_Z$ [74–76]. There is a broad consensus that at pH 6.5 the stoichiometry for the proton release from the water oxidizing complex into the bulk is close to 1, 0, 1, 2 protons in the S$_0 \rightarrow$ S$_1$, S$_1 \rightarrow$ S$_2$, S$_2 \rightarrow$ S$_3$ and S$_3 \rightarrow$ S$_0$ transitions, respectively, *e.g.* [77–82]. In wild-type PSII, after increasing the pH, the ability of the S$_2^{HS}$-state to progress to S$_3$ at 198 K was suggested to be due to the S$_2^{HS}$-state being deprotonated [26]. It was further suggested [26] that the increase of pH mimics the electrostatic influence of Tyr$_Z$·(His$^+$) on the S$_2^{LS} \leftrightarrow$ S$_2^{HS}$ equilibrium when the enzyme function at low pH values. In this model, we could predict that at high pH values the proton release that normally occurs in the S$_2$ to S$_3$ transition would occur on the S$_1$ to S$_2$ transition. Since in the V185T mutant the S$_2^{HS}$ configuration was observed without increasing the pH value and since the efficiency of S$_2^{HS}$ formation was greater when the state was generated at room temperature it seems indeed possible that the pattern of the proton release is modified by the V185T mutation. This hypothesis has been investigated by measuring the absorbance changes of the indicator dye bromocresol purple as previously described for Sr/Br-WT*3-PSII [64].

Firstly, the time-resolved flash dependence of the proton release was investigated in Ca/Cl-WT*3-PSII, something that has not yet been reported in the literature for PSII from *T. elongatus* with this procedure. Fig. 11 shows the absorption changes at 575 nm which are associated with changes in the protonation state of bromocresol purple, after flashes given to a dark-adapted WT*3-PSII (Panel A). At 575 nm, the unprotonated form of the dye has the largest extinction coefficient so that a light-induced decrease in absorbance reflects a proton release by PSII. The kinetics shown in Fig. 11 were recorded after the first flash (black), the second flash (red), the third flash (blue) and fourth flash (green).

After the first flash, *i.e.* in the S$_1$Tyr$_Z$· to S$_2$Tyr$_Z$ transition, no proton release was expected to occur (see above). Instead, the data show that there was a proton uptake occurring in two different time ranges. The slowest one, starting approximately 20 ms after the flash illumination, and already seen previously [64], has an unknown origin. It was proposed to possibly result from reactions involving the added electron acceptors. Alternatively, it could correspond to a drift in the base line that is unavoidable for such long time range. Fortunately, as previously described [64], it occurs on all flashes with the same amplitude and it can therefore be easily subtracted (see the Supplementary material). The fastest proton uptake very likely corresponds to the reduction of the

non-heme iron by Q$_A^-$ in centers in which the iron was oxidized prior to the flash [64]. In WT*3-PSII, this proton uptake occurred mainly on the first flash because the non-heme iron had no time to be reoxidized between the flashes under the conditions used here.

After the second flash, *i.e.* in the S$_2$Tyr$_Z$· to S$_3$Tyr$_Z$ transition, a proton release was now detected with a $t_{1/2}$ close to 30–40 μs. Data at 575 nm in Fig. 11 and those at 292 nm in Fig. 6 cannot be compared after the second flash because at 292 nm the absorption of the S$_2$Tyr$_Z$· and S$_3$Tyr$_Z$ states are too close so that almost no absorption changes are detectable. The fast proton release observed after the 2nd flash illumination was then followed by the slow proton uptake described above.

After the third flash, 2 different proton release kinetics were observed. A fast one with a $t_{1/2}$ of ≈ 20 μs occurring during the lag phase observed at 292 nm and a slowest one with $t_{1/2} \approx$ 1–2 ms similar to the S$_3$Tyr$_Z$· to S$_0$Tyr$_Z$ transition measured at 292 nm and to the O$_2$ release measured with the rate electrode. These proton releases are then followed by the slow proton uptake described above.

In contrast to the measurement at 292 nm which does not allow the resolution of the S$_0$Tyr$_Z$· to S$_1$Tyr$_Z$ transition, a proton release was observed after the fourth flash. The $t_{1/2}$ of this proton release was ≈ 200 μs that was totally different from that measured on the 3rd flash thus showing that it was not due to the S$_3$Tyr$_Z$· to S$_0$Tyr$_Z$ transition in centers still in S$_3$ after the 3rd flash due to the misses. The $t_{1/2} \approx$ 200 μs for the proton release measured here in the S$_0$Tyr$_Z$· to S$_1$Tyr$_Z$ transition was approximately 4 times slower than the electron transfer rate [66]. To our knowledge, these data constitute the first direct measurement of the time-resolved proton release in this transition.

The rough data in the WT*3-PSII described above are clear enough to be interpreted without additional treatments. However, for the analysis of the data in the V185T-PSII such refinement will be useful. This treatment is explained in detail in the Supplementary material. In WT*3-PSII, it mainly consisted in the subtraction of the slow uptake contribution which occurred on all flashes. Panel C in Fig. 11 shows the result of such a subtraction. A remaining small fast proton uptake is now detectable on the second flash indicating that the reduction of the non-heme iron was probably not complete on the first flash. By comparing the amplitude of the ΔI/I changes, the stoichiometry for the proton release in WT*3-PSII, at pH 6.3, appeared very close to the well-known 1,0,1,2 pattern for the S$_0$Tyr$_Z$· → S$_1$Tyr$_Z$, S$_1$Tyr$_Z$· → S$_2$Tyr$_Z$, S$_2$Tyr$_Z$· → S$_3$Tyr$_Z$ and S$_3$Tyr$_Z$· → S$_0$Tyr$_Z$ transitions, respectively.

Panel B in Fig. 11 shows the kinetically resolved proton uptake and proton release in the V185T-PSII. A similar analysis to that done above in WT*3-PSII was used for the mutant. After the first flash, *i.e.* in the
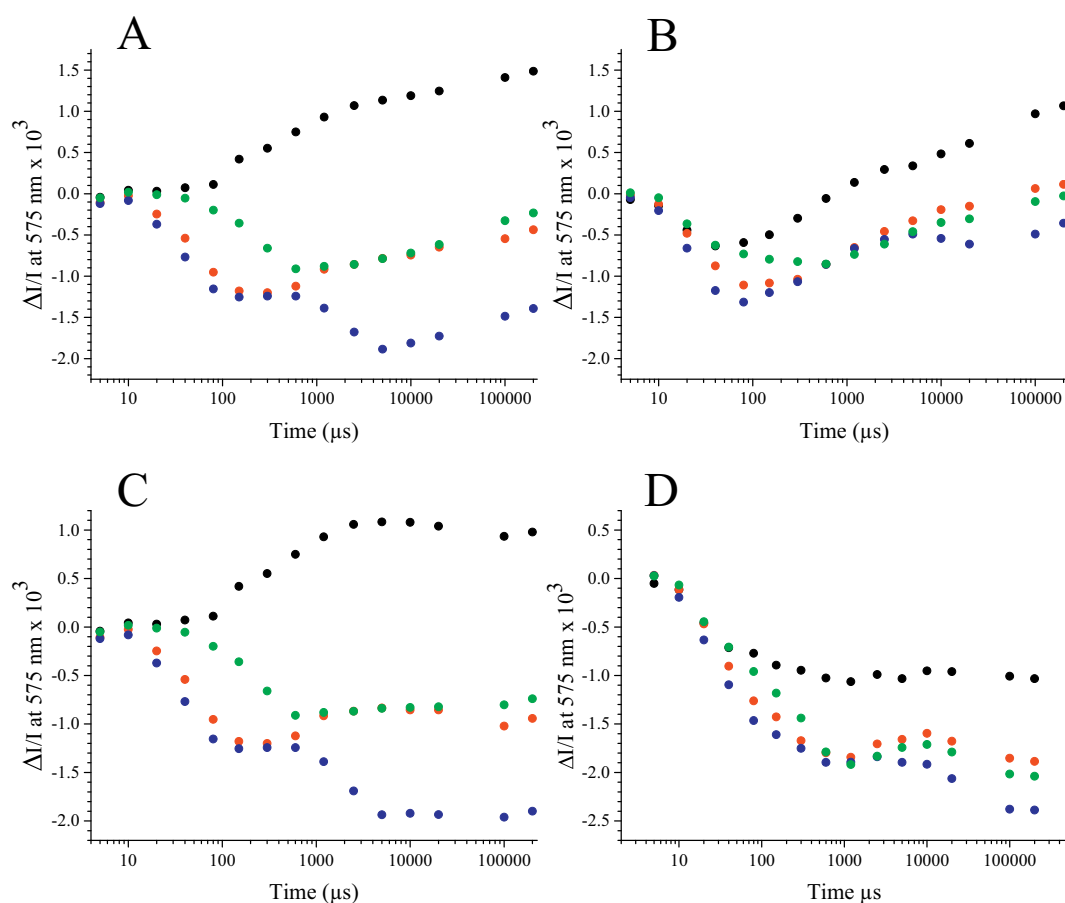
Fig. 11. Time-courses of the absorption changes at 575 nm after the first flash (black points), the second flash (red points), the third flash (blue points), and the fourth flash (green points) given to dark-adapted WT*3-PSII (Panel A) and V185T-PSII (Panel B) given to dark-adapted PSII samples in the presence of 150 μM bromocresol purple, 100 μM PPBQ and 100 μM ferricyanide. Panels C and D show the corrected time courses of the absorption changes by subtracting the apparent proton uptake which occurs in all S-state transitions as described in the Supplementary material. (For interpretation of the references to colour in this figure legend, the reader is referred to the web version of this article.)

$S_1Tyr_Z\cdot$ to S_2Tyr_Z transition, a fast decrease in the absorption was observed thus showing that in contrast to the WT*3-PSII there was a proton release in this transition. The origin of this proton will be discussed thereafter. Then, as in WT*3-PSII, there was a proton uptake occurring in two different time ranges. One after 20 ms, with a similar kinetics to that in the WT*3 sample and a faster one similar to that of the proton uptake corresponding to the reduction of the non-heme iron by Q_A^-.

On the second flash, *i.e.* in the $S_2Tyr_Z\cdot$ to S_3Tyr_Z transition, there was a proton release followed by the two kinetically distinct uptakes. It appears that, in contrast to the WT*3-PSII sample, these two uptakes were observed on all flashes in the mutant. This suggests that the proportion of centers in which the non-heme iron was reoxidized between the flashes under the conditions used was larger in the V185T mutant. Indeed, EPR controls confirmed that the proportion of oxidized non-heme iron could be larger in the V185T-PSII (not shown).

On the third flash, two kinetically proton releases were observed. The faster one occurring during the lag phase observed at 292 nm and a slower one with a $t_{1/2} \approx 20$ ms similar to that of the $(S_3Tyr_Z\cdot)'$ to S_0Tyr_Z transition measured at 292 nm. A proton release significantly slower than the fast one observed after the 2nd and 3rd flash was also detectable after the 4th flash.

As described in the Supplementary material, we tentatively subtracted the "uptake" contributions and the result is shown in Panel D of Fig. 11. Although the result is not perfect, mainly on the second flash, the proton release stoichiometry and the kinetics are identifiable on each of the 4 flashes. Except for the differences in the kinetics, another

important change between WT*3-PSII and V185T-PSII was the detection of a proton release after the first flash in the latter. Two different origins can be proposed for this proton: i) a proton associated with the formation of the S_2-state and ii) an electrostatically triggered proton release induced by the Tyr_Z oxidation [83] in a proportion of V185T-PSII that are Mn-depleted. It has been shown [83] that the kinetics for the proton release in inactive PSII was slightly slower (approximately two times) upon Tyr_Z oxidation than in active PSII. This is exactly was we also observed by comparing the release on the first flash to that in Mn-depleted PSII (see Supplementary material). Although we cannot rule out the contribution of dead centers in the data reported in Panels C and D in Fig. 11, it seems likely that active centers also contributed in the proton release observed on the first flash and we tentatively attribute this proton release to centers in which the S_2^{HS}-state is formed by the 1 flash illumination. The fast proton release in the $S_2Tyr_Z\cdot$ to S_3Tyr_Z transition seen in all the centers in WT*3-PSII and in centers in which a S_2^{LS} is formed after the 1 flash illumination in the V185T-PSII is attributed to the $S_2^{LS}Tyr_Z\cdot$ to $S_2^{HS}Tyr_Z\cdot$ transition. The consequence is that the proton release with a $t_{1/2}$ of 30 μs and detected in the $S_2^{LS}Tyr_Z\cdot$ to S_3 transition in WT*3-PSII at pH 6.5 occurred in the $S_2^{LS} \rightarrow S_2^{HS}$ transition triggered by the formation of $Tyr_Z\cdot$.

Calculations have predicted that the S_2^{LS} and S_2^{HS} configuration in wild-type PSII are close in energy at room temperature [35,84–86]. Such energy levels could be in principle experimentally probed by recording the themoluminescence [87,88] after one flash given at different pH values. Unfortunately, varying the pH has several effects on the TL emission mainly by affecting the protonation state of the
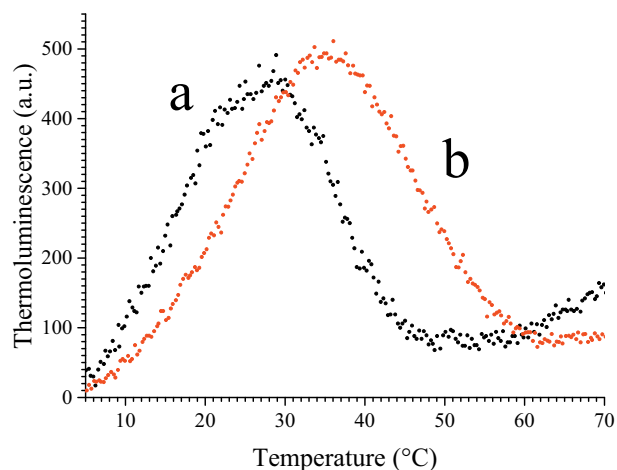
Fig. 12. Thermoluminescence glow curves from $S_2Q_A^-$/DCMU charge recombination measured after one flash given at 0 °C in WT*3-PSII (curve a) and V185T-PSII (curve b). The samples were previously dark-adapted at room temperature for 1 h before being loaded into the cuvette and illuminated. The heating rate was 0.6 °C/s.

acceptor side [89]. Here, we used the property of the V185T mutant which exhibits a high proportion of centers in the S_2^{HS} configuration at a pH value where all the centers are in S_2^{LS} configuration in the WT*3-PSII with the hope to get round this problem. Fig. 12 shows the thermoluminescence curves for the $S_2Q_A^-$ charge recombination after one flash in the presence of DCMU which blocks the forward electron transfer from Q_A^- to Q_B in WT*3-PSII (curves a, black) and V185T-PSII (curves b, red). A slightly higher peak temperature was observed in the V185T-PSII mutant which is indicative of a slightly lower energy level [87,88] for S_2 assuming no changes on the acceptor side in V185T-PSII. This was deduced from fluorescence decay measurements in the V185N-PSII mutant in *Synechocystis* 6803 [52] even if minor changes on the acceptor side cannot be totally ruled out since, for example, we already saw that the Ca/Sr exchange affected also the E_m of the Q_A^-/Q_A couple [90]. However, these possible effects on the acceptor side did not result in significantly different fluorescence decay [52].

An enhancement of the thermoluminescence emission is expected to accompany a higher peak temperature. However, as previously discussed [88], this enhancement can be small as observed in Fig. 12. By measuring the $S_2Q_A^-$ charge recombination after 1 flash in the presence of DCMU at different heating rates (not shown) it has been found that the proportion of non-radiative charge recombination by the direct and/or indirect routes was not modified in the mutant. According to the empirical relationship between the shift in free energy and in the peak temperature [87,88], *i.e.* ≈ + 0.6 °C/mV, the upshift of the peak temperature in V185T-PSII by approximately ≈ 8 °C, from 27 °C to 35 °C, would correspond to a decrease in the free energy level in the mutant by ≈ 13 mV. Such result is in agreement with the theoretical works mentioned in the introduction since the presence of a deprotonated HS configuration has only a minor effect on the free energy level of S_2.

4. Discussion

Valine 185 of the D1 subunit has been shown to be a key amino acid residue in the mechanism of O_2 evolution [41,44,52,54]. In *Synechocystis* 6803, mutation of this residue into asparagine dramatically slowed down the two steps $S_3Tyr_Z\cdot \rightarrow (S_3Tyr_Z\cdot)' \rightarrow S_0Tyr_Z + O_2$. The proximity of the chloride with V185 led the authors [52] to propose an alteration of the halide environment upon the mutation of V185 together with perturbations of both the H-bond network and the water molecules close to O5 [54] that is proposed to be one of the substrate water molecules [29,35,36,91]. As mentioned in some theoretical papers [92,93], the original DFT studies analyzing the water insertion in

the S_2 to S_3 transition into the Mn_4CaO_5 cluster [36] did not take into account that the V185 residue could be a hindrance for water binding to the Mn1. Further computational works suggested that V185 needed to rotate to allow the binding of the water molecule to Mn1 [93]. In the present work, the role of V185 has been further experimentally investigated by studying the PSII properties of a V185T mutant in the thermophilic cyanobacterium *T. elongatus*.

The V185T mutant in *T. elongatus* was able to grow photoautotrophically despite the strong alteration of the PSII function. The data in Fig. 3 show that the PSII polypeptide profile was not modified in the mutant thus showing that these alterations were not due to the loss of polypeptides, at least these subunits that are in the detection range of a polyacrylamide gel electrophoresis. As in the V185N mutant in *Synechocystis* 6803, the V185T mutation in *T. elongatus* strongly slowed down the O_2 evolution both under continuous illumination and flash illumination. From a theoretical activity of 6000 μmol O_2 (mg Chl)$^{-1}$ h^{-1}, which corresponds to ≈ 50 O_2 molecules evolved per PSII and 2 Q_B/Q_BH_2 exchanges per second, one can infer that the limiting step for 1 O_2 evolved takes 20 ms. This value is much larger than the lifetime found for the $S_3Tyr_Z\cdot$ to S_0Tyr_Z transition in WT*3 samples. In contrast, in V185T-PSII, the slowness of the $S_3Tyr_Z\cdot$ to S_0Tyr_Z transition measured under flash illumination in Fig. 4C with a $t_{1/2} \approx 20$ ms is expected to translate into a decrease of the O_2 evolution activity under continuous illumination. The simulated O_2 evolution in Fig. 4D shows that this slow down fits relatively well with the decrease by a factor ≈ 4 of the amplitude of the O_2 evolution under flash illumination in the V185T thylakoids measured in Fig. 4B when compared to the WT*3-thylakoids in Fig. 4A. In contrast to the situation in *Synechocystis* 6803 V185N mutant [52], the oscillations were also severely damped thus suggesting that other S-state transitions could be affected in the *T. elongatus* V185 T mutant. This was investigated by measuring the flash induced absorption changes at 292 nm. The damping of the oscillation with a period four in the V185T-PSII appeared much less severe than in the flash O_2 measurement reported in Panel B of Fig. 4 for V185T-thylakoids. This is not totally unexpected because the presence of an electron acceptor in the experiment reported in Fig. 5 which rapidly oxidizes the reduced quinones, may prevent the charge recombination that can occur during the long lifetime of the $S_3Tyr_Z\cdot$ state in the mutant.

The data in Fig. 6 show that the V185T mutation has strong consequences on the kinetics of the two $S_3Tyr_Z\cdot \rightarrow (S_3Tyr_Z\cdot)' \rightarrow S_0Tyr_Z + O_2$ transitions and to a less extent on the $S_1Tyr_Z\cdot \rightarrow S_2Tyr_Z$ transition (kinetics data are summarized in a table in the Supplementary material). The $t_{1/2}$ found at 292 nm for the $S_3Tyr_Z\cdot \rightarrow (S_3Tyr_Z\cdot)'$ transition, ≈ 1–2 ms instead of 100–200 μs in WT*3-PSII, and $(S_3Tyr_Z\cdot)' \rightarrow S_0Tyr_Z$ transition, ≈ 20 ms instead of 1–2 ms in WT*3-PSII, are in good agreement with the rate of O_2 evolution measured in Fig. 4 with thylakoids although the artefact at the shortest times with the rate electrode, see also Ref. [52], did not allow us to precisely estimate the lag-time. The increase in the $t_{1/2}$ of the $S_1Tyr_Z\cdot \rightarrow S_2Tyr_Z$ transition from ≈ 50 μs in WT*3-PSII to ≈ 100–150 μs in V185T-PSII may contribute to the decrease of the activity of the mutant by favoring the probability of a $Tyr_Z\cdot Q_A^-$ charge recombination in the S_1-state even in the presence of added electron acceptors. From QM/MM calculations [91], Val185 has also been proposed to play a key role in the S_4 to S_0 transition in the initial O_2 release process by acting as a hydrophobic one-way gate to transfer only O_2 from the active site to the O_2 channel and in the further water insertion. The data above show that the V185T mutation affects to same extent the kinetics of the O_2 release and the reduction kinetics of the Mn_4CaO_5 cluster.

Some of the structural consequences of the V185T mutation have been probed by recording the EPR spectra of the S_2-state and S_3-state both in the Ca-containing and Sr-containing mutant PSII (Figs. 7 and 8). Several observations could be done. Firstly, the Ca-V185T-PSII and the Sr-V185T-PSII exhibited a high proportion of S_2 in a high spin configuration. Secondly, both the S_2^{LS} and S_2^{HS} states have their EPR

properties modified when compared to the WT*3-PSII thus showing that the modifications of the environment of the Mn$_4$-cluster induced by the V185T mutation affect the magnetic couplings inside the cluster. The high proportion of S$_2^{HS}$ state was observed at a pH value at which the activity of PSII is close to the maximum (Fig. 10). This contrasts with the situation in Ca-WT*3-PSII in which the S$_2^{HS}$ configuration is observed only at pH ≥ 8.0, something explained with a model in which a deprotonation of the S$_2^{LS}$-state triggers the formation of the S$_2^{HS}$-state [26]. The observation of a high proportion of the S$_2^{HS}$ at pH 6.5 implies that the pK_a of the group(s) which deprotonate(s) in the S$_2^{LS}$ to S$_2^{HS}$ transition are significantly lowered by the V185T mutation thus confirming that the V185T mutation perturbs the large H-bond network around the Mn$_4$CaO$_5$ cluster. Among the groups identified as possibly being subject to this deprotonation they are W1, W2, W3, W4, D61, H332 and H337 [26]. In agreement with this suggestion, it has been recently shown [44] that in *Synechocystis* 6803 the V185N mutation altered the environments of the carboxylate groups whose the pK_a values change in the S$_1$ to S$_2$ transition. Thirdly, the S$_2^{HS}$ was formed both by a flash illumination at room temperature and by illumination at 198 K, whereas in Ca-WT*3-PSII the formation of the S$_2^{HS}$-state was not detected at any pH value, when the S$_2$-state was induced by low temperature illumination. However, in both the Ca-V185T-PSII and the Sr-V185T-PSII, whereas the amplitudes of the S$_2^{LS}$ multiline signals induced by either 1 flash at room temperature or an illumination at 198 K were similar, the amplitude of the S$_2^{HS}$ signals were significantly larger after the flash illumination rather than the illumination at 198 K. Usually, larger S$_2$ signals are observed when the S$_2$-state is induced by continuous illumination at 198 K rather than by flash illumination at room temperature because the miss parameter does no longer contribute to the decrease of the yield of the S$_2$ formation. This result therefore suggests that, in the V185T-PSII, the temperature dependence efficiency of the S$_1$ to S$_2$ transition differs from that in WT*3-PSII. To rationalize these observations, a model can be proposed in which the group(s) whose the deprotonation trigger(s) the S$_2^{LS}$ to S$_2^{HS}$ transition has(have) an apparent pK_a close to 6.5, instead of 8.3 in Ca-WT*3-PSII [26], and in which this(these) group(s) is(are) already deprotonated in a fraction of centers, approximately half, in the S$_1$-state. In the population of centers in which these groups are not deprotonated, the S$_1$ to S$_2$ transition would be blocked at 198 K. As the deprotonation discussed here has been shown to occur only at temperatures ≥ 230 K [30], the formation of a small proportion of S$_2$ in the HS configuration upon an illumination at 180 K of Sr-WT*3-PSII already led us to suggest that, in some centers, such a deprotonation could occur in the S$_1$-state [30]. Finally, to explain why some centers do not progress to S$_2$ at 198 K in the V185T mutant it can be proposed that in the mutant the S$_2^{HS}$-state is formed directly from S$_1$ without the formation of the S$_2^{LS}$-state as an intermediate. The model described above implies that a deprotonation event is required in the S$_1$ to S$_2$ transition in the V185T mutant. This was addressed by measuring proton releases under flash illumination by using bromocresol purple, at 575 nm, as a pH sensitive dye. At this wavelength, the protonated form of the dye has the smallest extinction coefficient so that a light-induced decrease in absorbance reflects a proton release by PSII and the light-induced increase in the absorbance reflects a proton uptake by PSII.

Several different approaches concurred in establishing the proton pattern release: sensitive glass electrode [78,81], absorption changes of pH-responding dyes [77,79,81] and isotope-edited infrared spectroscopy [80]. Alternative methods have been also used that do not probe directly changes in H$^+$ concentration in the bulk phase, but the consequences of the proton release in terms of charges distribution within the protein, using electrochromic bandshift [79], or in terms of free enthalpy change by time-resolved photothermal beam deflection [75]. These time resolved measurements evidenced the release of one proton per PSII in the S$_0$Tyr$_Z$• → S$_1$Tyr$_Z$ and in the S$_2$Tyr$_Z$• → S$_3$Tyr$_Z$ transitions and one proton in each of the two S$_3$Tyr$_Z$• → (S$_3$Tyr$_Z$•)′ → S$_0$Tyr$_Z$ transitions.

All the events affecting the concentration of protons in the bulk and which are expected to occur in the WT*3-PSII and V185T-PSII samples are clearly identifiable in Fig. 11. Moreover, the oscillating pattern of the absorption changes at 575 nm after each flash was similar to that at 292 nm thus showing that the proton release pattern follows the S-state cycle (not shown). In WT*3-PSII, in the S$_1$Tyr$_Z$• → S$_2$Tyr$_Z$ transition (1st flash) no proton release was observed in agreement with the literature. Instead, a proton uptake was observed in the time range corresponding to the reduction of the non-heme iron by Q$_A^-$ [11,64]. The non-heme iron is indeed oxidized in a proportion of centers in dark-adapted *T. elongatus* PSII samples, *e.g.* [11]. Upon its reduction by Q$_A^-$, the reoxidation has no time to occur between the flashes (300 ms apart) [64] so that it contributes mainly on the first flash. The very small uptake observed on the 2nd flash in Fig. 11A and B can be reasonably attributed to the same non-heme iron reduction in the centers in which it was not reduced after the first flash due to the misses which are close to 10% in this material [58]. In the S$_2$Tyr$_Z$• → S$_3$Tyr$_Z$ transition (2nd flash) a proton release was detected with a $t_{1/2}$ close to 30–40 μs. This $t_{1/2}$, which is in very good agreement with previous measurements [75,94], is approximately 10 times smaller than the $t_{1/2}$ of the electron transfer reported in the literature for this transition, *i.e.* ≈ 300 μs [66,94,95]. Interestingly, a complex time-resolved infrared signal has been observed in the time range of the proton release before the rise intensity in the trace of the reduced Tyr$_Z$ [96]. Therefore, we propose that this proton release occurs in the S$_2^{LS}$ to S$_2^{HS}$ transition triggered by the formation of Tyr$_Z$• prior to the electron transfer from the S$_2^{HS}$-state to Tyr$_Z$•. After the 3rd flash, a proton release was observed with two distinct kinetic phases. The fast one, ended after ≈ 100 μs, corresponds to the proton releases in the S$_3$Tyr$_Z$• → (S$_3$Tyr$_Z$•)′ transition seen as a lag phase in absorption change measurements at 292 nm (Fig. 6A) in agreement with previous measurements [97]. The slow one occurred with a $t_{1/2}$ close to 1.5 ms and corresponds to the (S$_3$Tyr$_Z$•)′ → S$_0$Tyr$_Z$ transition also seen at 292 nm (Fig. 6A) and in O$_2$ measurements with the rate electrode (Fig. 4). Finally, after the 4th flash, a proton release was detected. The time-resolved signal observed on the 4th flash differs significantly enough from that observed after the 1st, 2nd and 3rd flashes to be certain that it does not originate from contributions to other transitions that would be due to misses. The $t_{1/2}$, close to 200 μs, is in the time range of the electron transfer reported for this transition in plant PSII, *i.e.* ≈ 250 μs [74], but slightly differs from the photothermal beam deflection signal reported in this transition with a $t_{1/2}$ close to 30 μs attributed to a pure electron transfer from the cluster to Tyr$_Z$• and a $t_{1/2}$ close to 100 μs associated to the proton release following the oxidation of the cluster [97]. Finally, the amplitudes of the ΔI/I induced by each of the four flashes at pH 6.3 are well in agreement with the 1, 0, 1, 2 stoichiometry for the S$_0$Tyr$_Z$• → S$_1$Tyr$_Z$, S$_1$Tyr$_Z$• → S$_2$Tyr$_Z$, S$_2$Tyr$_Z$• → S$_3$Tyr$_Z$ and S$_3$Tyr$_Z$• → S$_0$Tyr$_Z$ transitions, respectively [77–82].

In the V185T-PSII samples, the flash dependence of the proton release shown in Fig. 11B differs significantly from that in the WT*3-PSII. In this experiment, we cannot discard the contribution of dead centers on each flash (see the discussion in the Results section). However, the analysis of the data indicates that a large part of the signal originates from active centers. The EPR results have shown that a large proportion of centers in the S$_2^-$ state are in the HS configuration after a flash illumination at room temperature. We propose that the groups which govern the S$_2^{LS}$ to S$_2^{HS}$ transition by favoring the proton release from W1 when S$_2$Tyr$_Z$• is formed have their pK_a modified by the V185T mutation so that the deprotonation of W1 already occurs in the S$_2^{LS}$Tyr$_Z$• state. In other words, in the V185T mutant, the S$_2^{LS}$ to S$_2^{HS}$ would occur without the need to oxidize Tyr$_Z$. In agreement with this model, a fast proton release is observed after the first flash in the V185T-PSII (Fig. 11B). Maybe relevant to this observation is that the pH value at which the EPR experiments have been done, *i.e.* 6.5, was slightly above the optimum pH value for O$_2$ evolution in the V185T-PSII sample, *i.e.* 6.0. This could be a situation analogous to that in WT*3-

PSII in which increasing the pH value favors the S_2^{HS} configuration. The question of the pH dependence of the S_2^{LS} to S_2^{HS} transition in the V185T-PSII will be addressed in future studies.

After the 3rd flash, a proton release was observed with two distinct kinetic phases. The fast one, ended after ≈ 1 ms instead of $\approx 100\,\mu s$ in WT*3-PSII, is in very good agreement with the increase in the duration of the lag time in the V185T-PSII corresponding to the $S_3 Tyr_Z\cdot \rightarrow (S_3 Tyr_Z\cdot)'$ transition seen as a lag phase in absorption change measurements at 292 nm. The slow one occurred with a $t_{1/2}$ close to ≈ 20 ms, instead of ≈ 1.5 ms in WT*3-PSII, and corresponds to the $(S_3 Tyr_Z\cdot)' \rightarrow S_0 Tyr_Z$ transition also seen at 292 nm (Fig. 6B) and in O_2 measurements with the rate electrode (Fig. 4). It is more difficult to estimate the kinetic rates and amplitudes after the 2nd and 4th flashes. The amplitude of the absorption change due to an electrostatically triggered proton release induced by the Tyr_Z oxidation in Mn-depleted PSII would be larger, but kinetically distinct, than the absorption change due the release of one proton in active centers [98]. However, after the 2nd and 4th flash, the kinetics of the proton release in the V185T-PSII in the $S_2^{LS} Tyr_Z\cdot \rightarrow S_3 Tyr_Z$ and $S_0 Tyr_Z\cdot \rightarrow S_1 Tyr_Z$ transitions, respectively, seem comparable to those observed in WT*3-PSII.

If we neglect the misses, 4 protons should be released in a sequence of 4 flashes. The release of a proton in a proportion of centers in the $S_1 Tyr_Z\cdot \rightarrow S_2 Tyr_Z$ transition in the V185T-PSII implies that in the same centers there is a deficit in the proton release in another transition. From the data in Fig. 11 it is difficult to identify this transition. However, the slow release in the $(S_3 Tyr_Z\cdot)' \rightarrow S_0 Tyr_Z$ transition in the V185T-PSII seemed to have a slightly smaller amplitude than in the WT*3-PSII. However, it is interesting to note that in the most intact plant PSII and at high pH where a proton release was observed after the first flash [79,99] a release that we attribute here to the high pH induced S_2^{LS} to S_2^{HS} conversion [26], a deficit was observed either on the $S_0 \rightarrow S_1$ transition [79] or on the $S_3 \rightarrow S_0$ transition [99]. Future works will be useful to clarify this point. It is worth mentioning that the pH dependence of the lag phase $S_3 Tyr_Z\cdot \rightarrow (S_3 Tyr_Z\cdot)'$ observed in wild type PSII from *Synechocystis* 6803 was abolished in the V185N mutant [54]. This effect could contribute in part to the different pH dependence of O_2 evolution in the wild-type PSII and the mutant PSII. In addition, the specific effect of the mutation of the V185 on the pH dependence of the $S_3 Tyr_Z\cdot \rightarrow (S_3 Tyr_Z\cdot)'$ step indicates that the proton released in this transition used a different path than in wild-type PSII possibly involving groups that are not titrated in the pH range studied.

The EPR spectroscopy and oxygen evolution measurements under continuous illumination have shown that the V185T mutant was able to biosynthetically incorporate bromide instead of chloride and strontium instead of calcium. The pH dependence of O_2 evolution in the V185T-PSII shows that the S_2^{HS} configuration is observed at a pH value that is very close to the optimum for the O_2 activity in contrast to WT*3-PSII. The opposite effects of the halide exchange on the pH dependency in WT*3-PSII and V185T-PSII is an experimental evidence supporting a previous suggestion that the halide binding site and the V185 residue interact [52].

The amplitude of the S_3 signal generated by 2 flashes given at room temperature appeared slightly smaller in Sr-V185T-PSII that in Ca-V185T-PSII (Fig. 8). A possible explanation for such a difference in the amplitudes is given in the following. The S_3-state is found to be heterogeneous with: *i*) the $S = 3$ form shown in Fig. 8 and not sensitive to near-infrared light; and *ii*) a form that is not EPR visible but in which Mn-photochemistry occurs resulting in the formation of a $(S_2 Y_Z\cdot)'$ split EPR signal upon near-infrared illumination at helium temperatures (*e.g.* 4.2 K) [30,33,70]. Upon near-infrared illumination any $(S_2 Y_Z\cdot)'$ split EPR signal could be induced in the Ca-V185T-PSII in contrast to the Sr-V185T-PSII in which a NIR-induced split signal was observed (not shown). Taken together, these two observations suggest that the lack of NIR sensitivity of the S_3-state and the larger amplitude of the $S = 3$ S_3 signal in the Ca-V185T-PSII originate from a structural change of the Mn_4CaO_5 resulting into the conversion of centers with an EPR invisible

S_3-state in Sr-V185T-PSII into centers exhibiting the $S = 3$ S_3 signal in Ca-V185T-PSII.

Whereas both the S_2^{LS} and S_2^{HS} EPR signals are modified by the Ca/Sr exchange, the S_3 EPR signal remained unaffected. We already reported that the Ca/Sr exchange had also no effect on the S_3 signal in WT*3-PSII [26]. These results show that the configuration of the Mn_4 cluster is much less flexible in the S_3-state than in the S_2-state and possibly than in the S_1-state. This is not surprising since the S_3-state is the precursor of the state in which the O_2 formation occurs *i.e.* the state where probably a single configuration allows the reaction to occur. This observation implies that the slowdown of the $S_3 Tyr_Z\cdot \rightarrow S_0 Tyr_Z$ transition has either a thermodynamic origin as in the case of the Ca/Sr exchange which decreases the entropic part of the reaction [33] and/or originate from structural modifications around the cluster, as structural relaxations of the protein, that affect the H-bond network without significantly modifying the structure of the cluster in agreement with previous works [44,54].

Finally, the presence of a high proportion of S_2^{HS} in the V185T-PSII allowed us to show that *i*) the S_2^{HS} to S_3 transition may also occur at 198 K at a low pH value and *ii*) the S_1 to S_2^{HS} transition is less efficient at low temperature than at room temperature, in agreement with the model proposed above in which the S_2^{HS} formation is accompanied by a spontaneous proton release.

5. Conclusions

The study of the site directed mutant D1-V185T in *T. elongatus* allowed us to characterize to which extent the V185 amino acid is involved in the extensive H-bond network which tune the properties of the Mn_4CaO_5 cluster. For example, it is shown that the V185 and the chloride binding site very likely interact *via* this network. The V185 contributes to the stabilization of the S_2^{LS} configuration. In the V185T mutant a high proportion of the S_2^{HS} configuration is observed. A proton is very likely released in the $S_1 Tyr_Z\cdot \rightarrow S_2^{HS} Tyr_Z$ transition in the V185T mutant in contrast to the WT*3-PSII in which there is no proton release in this transition. Instead, in WT*3-PSII, a proton release kinetically distinct from the electron transfer is observed in the $S_2^{LS} Tyr_Z\cdot \rightarrow S_3 Tyr_Z$ transition and we propose that it occurs in the $S_2^{LS} Tyr_Z\cdot \rightarrow S_2^{HS} Tyr_Z\cdot$ intermediate state before the $S_2^{HS} Tyr_Z\cdot \rightarrow S_3 Tyr_Z$ transition. The dramatic slowdown of the $S_3 Tyr_Z\cdot \rightarrow S_0 Tyr_Z$ transition in the V185T mutant very likely does not originate from a structural modification of the cluster but more probably is indicative of less efficient relaxation processes of the H-bond network and/or the protein thus showing the important structural role of V185 in the PSII water splitting activity.

Transparency document

The Transparency document associated with this article can be found, in online version.

Appendix A. Supplementary data

Supplementary data to this article can be found online at https://

References

[1] M. Suga, F. Akita, K. Hirata, G. Ueno, H. Murakami, Y. Nakajima, T. Shimizu, K. Yamashita, M. Yamamoto, H. Ago, J.-R Shen, Native structure of photosystem II at 1.95 angstrom resolution viewed by femtosecond X-ray pulses, Nature 517 (2015) 99–103.

[2] J.-R. Shen, The structure of Photosystem II and the mechanism of water oxidation in photosynthesis, Annu. Rev. Plant Biol. 66 (2015) 23–48.

[3] F. Müh, M. Plöckinger, T. Renger, Electrostatic asymmetry in the reaction center of Photosystem II, J. Phys. Chem. Lett. 8 (2017) 850–858.

[4] H.G. Duan, V.I. Prokhorenko, E. Wientjes, R. Croce, M. Thorwart, R.J.D. Miller, Primary charge separation in the Photosystem II reaction center revealed by a global analysis of the two-dimensional electronic spectra, Sci. Rep. 7 (2017) 12347–12355.

[5] H. Dau, I. Zaharieva, M. Haumann, Recent developments in research on water oxidation by photosystem II, Curr. Opin. Chem. Biol. 16 (2012) 3–10.

[6] M. Perez-Navarro, F. Neese, W. Lubitz, D.A. Pantazis, N. Cox, Recent developments in biological water oxidation, Curr. Opin. Chem. Biol. 31 (2016) 113–119.

[7] D.J. Vinyard, G.W. Brudvig, Progress toward a molecular mechanism of water oxidation in Photosystem II, Annu. Rev. Phys. Chem. 68 (2017) 101–116.

[8] B.A. Diner, F. Rappaport, Structure, dynamics, and energetic of the primary photochemistry of Photosystem II of oxygenic photosynthesis, Annu. Rev. Plant Biol. 53 (2002) 551–580.

[9] C. Fufezan, C.-X. Zhang, A. Krieger-Liszkay, A.W. Rutherford, Secondary quinone in Photosystem II of Thermosynechococcus elongatus: semiquinone-iron EPR signals and temperature dependence of electron transfer, Biochemistry 44 (2005) 12780–12789.

[10] A. Sedoud, N. Cox, M. Sugiura, W. Lubitz, A. Boussac, A.W. Rutherford, The semiquinone-iron complex of Photosystem II: EPR signals assigned to the low field edge of the ground state doublet of $Q_A \cdot Fe^{2+}$ and $Q_B \cdot Fe^{2+}$, Biochemistry 50 (2011) 6012–6021.

[11] A. Boussac, M. Sugiura, F. Rappaport, Probing the quinone binding site of Photosystem II from Thermosynechococcus elongatus containing either PsbA1 or PsbA3 as the D1 protein through the binding characteristics of herbicides, Biochim. Biophys. Acta (2010) (1807) 119–129.

[12] B. Kok, B. Forbush, M. McGloin, Cooperation of charges in photosynthetic O_2 evolution–I. A linear four step mechanism, Photochem. Photobiol. 11 (1970) 457–475.

[13] P. Joliot, B. Kok, Oxygen evolution in photosynthesis, in: Govindjee (Ed.), Bioenergetics of Photosynthesis, Academic Press, New York, 1975, pp. 387–412.

[14] A. Boussac, A.W. Rutherford, Comparative study of the g = 4.1 EPR signals in the S_2-state of photosystem II, Biochim. Biophys. Acta 1457 (2000) 145–156.

[15] R. Pokhrel, G.W. Brudvig, Oxygen-evolving complex of photosystem II: correlating structure with spectroscopy, Phys. Chem. Chem. Phys. 16 (2014) 11812–11821.

[16] G.C. Dismukes, Y. Siderer, Intermediates of a polynuclear manganese center involved in photosynthetic oxidation of water, Proc. Natl. Acad. Sci. U. S. A. 78 (1981) 274–278.

[17] J.-L. Zimmermann, A.W. Rutherford, Electron Paramagnetic Resonance studies of the oxygen-evolving enzyme of Photosystem II, Biochim. Biophys. Acta 767 (1984) 160–167.

[18] J.L. Casey, K. Sauer, Electron Paramagnetic Resonance detection of a cryogenically photogenerated intermediate in photosynthetic oxygen evolution, Biochim. Biophys. Acta 767 (1984) 21–28.

[19] O. Horner, E. Rivière, G. Blondin, S. Un, A.W. Rutherford, J.-J. Girerd, A. Boussac, SQUID magnetization study of the infrared-induced spin transition in the S_2-state of photosystem II: spin value associated with the g = 4.1 EPR signal, J. Am. Chem. Soc. 120 (1998) 7924–7928.

[20] A. Boussac, S. Un, O. Horner, A.W. Rutherford, High spin states ($S \geq 5/2$) of the Photosystem II manganese complex, Biochemistry 37 (1998) 4001–4007.

[21] R.D. Britt, K.A. Campbell, J.M. Peloquin, J.L. Gilchrist, C.P. Aznar, M.M. Dicus, J. Robblee, J. Messinger, Recent pulsed EPR studies of the Photosystem II oxygen-evolving complex: implications as to water oxidation mechanisms, Biochim. Biophys. Acta 1655 (1655) (2004) 158–171.

[22] N. Cox, L. Rapatskiy, J.-H. Su, D.A. Pantazis, M. Sugiura, L. Kulik, P. Dorlet, A.W. Rutherford, F. Neese, A. Boussac, W. Lubitz, J. Messinger, The effect of Ca^{2+}/Sr^{2+} substitution on the electronic structure of the oxygen-evolving complex of Photosystem II: a combined multi-frequency EPR, 55Mn-ENDOR and DFT study of the S_2 state, J. Am. Chem. Soc. 133 (2011) 3635–3648.

[23] D.A. Pantazis, W. Ames, N. Cox, W. Lubitz, F. Neese, Two interconvertible structures that explain the spectroscopic properties of the oxygen-evolving complex of Photosystem II in the S_2 State, Angew. Chem. Int. Ed. 51 (2012) 9935–9940.

[24] D. Bovi, D. Narzi, L. Guidoni, The S_2 State of the oxygen-evolving complex of Photosystem II explored by QM/MM dynamics: spin surfaces and metastable states suggest a reaction path towards the S_3 State, Angew. Chem. Int. Ed. 52 (2013) 11744–11749.

[25] H. Isobe, M. Shoji, S. Yamanaka, Y. Umena, K. Kawakami, N. Kamiya, J.-R. Shen, K. Yamaguchi, Theoretical illumination of water-inserted structures of the CaMn₄O₅ cluster in the S_2 and S_3 states of oxygen-evolving complex of photosystem II: full geometry optimizations by B3LYP hybrid density functional, Dalton Trans. 41 (2012) 13727–13740.

[26] A. Boussac, I. Ugur, A. Marion, M. Sugiura, V.R.I. Kaila, A.W. Rutherford, The low spin - high spin equilibrium in the S_2-state of the water oxidizing enzyme, Biochim. Biophys. Acta 1859 (2018) 342–356.

[27] A. Boussac, M. Sugiura, A.W. Rutherford, P. Dorlet, Complete EPR spectrum of the S_3-state of the oxygen-evolving Photosystem II, J. Am. Chem. Soc. 131 (2009) 5050–5051.

[28] Y. Sanakis, J. Sarrou, G. Zahariou, V. Petrouleas, J.F. Allen, E. Gantt, J. Golbeck, B. Osmond, Recent EPR studies of the OEC of photosystem II. (A) Trapping tyrosyl Z · in action. (B) The critical S_3 integer-spin state of the Mn cluster in photosynthesis in energy from the Sun, 14th International Congress on Photosynthesis, Springer, Dordrecht, Netherlands, 2008, p. 479.

[29] N. Cox, M. Retegan, F. Neese, D.A. Pantazis, A. Boussac, W. Lubitz, Electronic structure of the oxygen evolving complex in Photosystem II prior to $O-O$ bond formation, Science 345 (2014) 804–808.

[30] A. Boussac, A.W. Rutherford, M. Sugiura, Electron transfer pathways from the S_2-states to the S_3-states either after a Ca^{2+}/Sr^{2+} or a Cl^-/I^- exchange in Photosystem II from Thermosynechococcus elongatus, Biochim. Biophys. Acta 1847 (2015) 576–586.

[31] N. Ioannidis, V. Petrouleas, Decay products of the S_3 state of the oxygen-evolving complex of photosystem II at cryogenic temperatures. Pathways to the formation of the S = 7/2 S_2 state configuration, Biochemistry 41 (2002) 9580–9588.

[32] V. Petrouleas, D. Koulougliotis, N. Ioannidis, Trapping of metalloradical intermediates of the S-States at liquid helium temperatures. Overview of the phenomenology and mechanistic implications, Biochemistry 44 (2005) 6723–6728.

[33] F. Rappaport, N. Ishida, M. Sugiura, A. Boussac, Ca^{2+} determines the entropy changes associated with the formation of transition states during water oxidation by Photosystem II, Energy Environ. Sci. 4 (2011) 2520–2524.

[34] M. Retegan, N. Cox, W. Lubitz, F. Neese, D.A. Pantazis, The first tyrosyl radical intermediate formed in the S_2-S_3 transition of photosystem II, Phys. Chem. Chem. Phys. (2014) 11901–11910.

[35] I. Ugur, A.W. Rutherford, V.R.I. Kaila, Redox-coupled substrate water reorganization in the active site of Photosystem II-The role of calcium in substrate water delivery, Biochim. Biophys. Acta 1857 (2016) 740–748.

[36] P.E.M. Siegbahn, Water oxidation mechanism in Photosystem II, including oxidations, proton release pathways, $O-O$ bond formation and O_2 release, Biochim. Biophys. Acta 1827 (2013) 1003–1019.

[37] H. Dau, M. Haumann, Time-resolved X-ray spectroscopy leads to an extension of the classical S-state cycle model of photosynthetic oxygen evolution, Photosynth. Res. 92 (2007) 327–343.

[38] C. Glockner, J. Kern, M. Broser, A. Zouni, V. Yachandra, J. Yano, Structural changes of the oxygen-evolving complex in Photosystem II during the catalytic cycle, J. Biol. Chem. 288 (2013) 22607–22620.

[39] R.J. Debus, FTIR studies of metal ligands, networks of hydrogen bonds, and water molecules near the active site Mn₄CaO₅ cluster in Photosystem II, Biochim. Biophys. Acta 1847 (2015) 19–34.

[40] T. Noguchi, Role of a water network around the Mn₄CaO₅ cluster in photosynthetic water oxidation: a Fourier transform infrared spectroscopy and Quantum Mechanics/Molecular Mechanics calculation study, Biochemistry 55 (2016) 597–607.

[41] H. Bao, P.L. Dilbeck, R. Burnap, Proton transport facilitating water-oxidation: the role of second sphere ligands surrounding the catalytic metal cluster, Photosynth. Res. 116 (2013) 215–229.

[42] K. Saito, A.W. Rutherford, H. Ishikita, Energetics of proton release on the first oxidation step in the water-oxidizing enzyme, Nat. Commun. 6 (2015) 8488.

[43] P.E.M. Siegbahn, Water oxidation energy diagrams for photosystem II for different protonation states, and the effect of removing calcium, Phys. Chem. Chem. Phys. 16 (2014) 11893–11900.

[44] C.J. Kim, H. Bao, R.L. Burnap, R.J. Debus, Impact of D1-V185 on the water molecules that facilitate O_2 formation by the catalytic Mn₄CaO₅ cluster in Photosystem II, Biochemistry 57 (2018) 4299–4311.

[45] R. Pokhrel, G.W. Brudvig, Oxygen-evolving complex of photosystem II: correlating structure with spectroscopy, Phys. Chem. Chem. Phys. 16 (2014) 11812–11821.

[46] R.J. Service, W. Hillier, R.J. Debus, Evidence from FTIR difference spectroscopy of an extensive network of hydrogen bonds near the oxygen-evolving Mn4Ca cluster of Photosystem II involving D1-Glu65, D2-Glu312, and D1-Glu329, Biochemistry 49 (2010) 6655–6669.

[47] R.J. Debus, Evidence from FTIR difference spectroscopy that D1-Asp61 influences the water reactions of the oxygen-evolving Mn₄CaO₅ cluster of Photosystem II, Biochemistry 53 (2014) 2941–2955.

[48] R.J. Service, W. Hillier, R.J. Debus, Network of hydrogen bonds near the oxygen-evolving Mn₄CaO₅ cluster of Photosystem II probed with FTIR difference spectroscopy, Biochemistry 53 (2014) 1001–1017.

[49] R. Pokhrel, R.J. Debus, G.W. Brudvig, Probing the effect of mutations of Asparagine 181 in the D1 subunit of Photosystem II, Biochemistry 14 (2015) 1663–1672.

[50] R. Nagao, H. Ueoka-Nakanishi, T. Noguchi, D1-Asn-298 in Photosystem II is involved in a hydrogen-bond network near the redox-active tyrosine Y_Z for proton exit during water oxidation, J. Biol. Chem. 292 (2017) 20046–20057.

[51] G. Banerjee, I. Ghosh, C.J. Kim, R.J. Debus, G.W. Brudvig, Substitution of the D1-Asn87 site in Photosystem II of cyanobacteria mimics the chloride-binding characteristics of spinach Photosystem II, J. Biol. Chem. 293 (2018) 2487–2497.

[52] P.L. Dilbeck, H. Bao, C.L. Neveu, R.L. Burnap, Perturbing the water cavity surrounding the manganese cluster by mutating the residue D1-Valine 185 has a strong effect on the water oxidation mechanism of Photosystem II, Biochemistry 52 (2013) 6824–6833.

[53] M. Sugiura, Y. Ozaki, M. Nakamura, N. Cox, F. Rappaport, A. Boussac, The D1-173 amino acid is a structural determinant of the critical interaction between D1-Tyr161 (TyrZ) and D1-His191 in Photosystem II, Biochim. Biophys. Acta 1837 (2014) 1922–1931.

[54] H. Bao, R.L. Burnap, Structural rearrangements preceding dioxygen formation by

the water oxidation complex of Photosystem II, Proc. Natl. Acad. Sci. U. S. A. 112 (2015) 6139–6147.

[55] M. Hundelt, A.-M. Hays, R.J. Debus, W. Junge, I.I. Oxygenic Photosystem, the mutation D1-D61N in *Synechocystis* sp. PCC 6803 retards S-state transitions without affecting electron transfer from YZ to P680, Biochemistry 37 (1998) 14450–14456.

[56] M. Sugiura, A. Boussac, T. Noguchi, F. Rappaport, Influence of Histidine-198 of the D1 subunit on the properties of the primary electron donor, P680, of Photosystem II in *Thermosynechococcus elongatus*, Biochim. Biophys. Acta 1777 (2008) 331–342.

[57] M. Sugiura, Y. Inoue, Highly purified thermo-stable oxygen evolving Photosystem II core complex from the thermophilic cyanobacterium *Synechococcus elongatus* having His-tagged CP43, Plant Cell Physiol. 40 (1999) 1219–1231.

[58] N. Ishida, M. Sugiura, F. Rappaport, T.-L. Lai, A.W. Rutherford, A. Boussac, Biosynthetic exchange of bromide for chloride and strontium for calcium in the Photosystem II oxygen-evolving enzyme, J. Biol. Chem. 283 (2008) 13330–13340.

[59] M. Ikeuchi, Y. Inoue, A new 4.8-kDa polypeptide intrinsic to the PS II reaction center, as revealed by modified SDS-PAGE with improved resolution of low-molecular weight proteins, Plant Cell Physiol. 29 (1988) 1233–1239.

[60] S. Styring, A.W. Rutherford, In the oxygen-evolving complex of Photosystem II the S0-state is oxidized to the S1-state by D+ (Signal-II slow), Biochemistry 26 (1987) 2401–2405.

[61] J.-M. Ducruet, Chlorophyll thermoluminescence of leaf discs: simple instruments and progress in signal interpretation open the way to new ecophysiological indicators, J. Exp. Bot. 54 (2003) 2419–2430.

[62] J.-M. Ducruet, I. Vass, Thermoluminescence: experimental, Photosynth. Res. 201 (2009) 195–204.

[63] D. Beal, F. Rappaport, P. Joliot, A new high-sensitivity 10-ns time-resolution spectrophotometric technique adapted to in vivo analysis of the photosynthetic apparatus, Rev. Sci. Instrum. 70 (1999) 202–207.

[64] H. Nilsson, F. Rappaport, A. Boussac, J. Messinger, Substrate-water exchange in Photosystem II is arrested prior to dioxygen formation, Nat. Commun. 5 (2014) 4305–4311.

[65] J. Lavorel, Determination of the photosynthetic oxygen release time by amperometry, Biochim. Biophys. Acta 1101 (1992) 33–40.

[66] F. Rappaport, M. Blanchard-Desce, J. Lavergne, Kinetics of electron-transfer and electrochromic change during the redox transitions of the photosynthetic oxygen-evolving complex, Biochim. Biophys. Acta 1184 (1994) 178–192.

[67] J. Lavergne, Improved UV-visible spectra of the S-transitions in the photosynthetic oxygen-evolving system, Biochim. Biophys. Acta 1060 (1991) 175–188.

[68] J.P. Dekker, H.J. van Gorkom, M. Brok, L. Ouwehand, Optical characterization of Photosystem II electron donors, Biochim. Biophys. Acta 764 (1984) 301–309.

[69] A. Boussac, N. Ishida, M. Sugiura, F. Rappaport, Probing the role of chloride in Photosystem II from *Thermosynechococcus elongatus* by exchanging chloride for iodide, Biochim. Biophys. Acta 1817 (2012) 802–810.

[70] N. Ioannidis, J.H.A. Nugent, V. Petrouleas, Intermediates of the S_3 state of the oxygen-evolving complex of Photosystem II, Biochemistry 41 (2002) 9589–9600.

[71] K.G.V. Havelius, J. Sjöholm, F.M. Ho, F. Mamedov, S. Styring, Metalloradical EPR signals from the $Y_Z \cdot$ S-state intermediates in Photosystem II, Appl. Magn. Reson. 37 (2010) 151–176.

[72] A. Boussac, F. Rappaport, K. Brettel, M. Sugiura, Charge recombination in $S_nTyr_Z \cdot$ $Q_A^- \cdot$ radical pairs in D1 protein variants of Photosystem II: Long range electron transfer in the Marcus inverted region, J. Phys. Chem. B 117 (2013) 3308–3314.

[73] A. Boussac, F. Rappaport, P. Carrier, J.-M. Verbavatz, R. Gobin, D. Kirilovsky, A.W. Rutherford, M. Sugiura, Biosynthetic Ca^{2+}/Sr^{2+} exchange in the photosystem II oxygen evolving enzyme of *Thermosynechococcus elongatus*, J. Biol. Chem. 279 (2004) 22809–22819.

[74] F. Rappaport, J. Lavergne, Coupling of electron and proton transfer in the photosynthetic water oxidase, Biochim. Biophys. Acta 1503 (2001) 246–259.

[75] A. Klauss, M. Haumann, H. Dau, Alternating electron and proton transfer steps in photosynthetic water oxidation, Proc. Natl. Acad. Sci. U. S. A. 109 (2012) 16035–16040.

[76] P.E.M. Siegbahn, M. Lundberg, The mechanism for dioxygen formation in PSII studied by quantum chemical methods, Photochem. Photobiol. Sci. 4 (2005) 1035–1043.

[77] S. Saphon, A.R. Crofts, Protolytic reactions in photosystem II - new model for release of protons accompanying photooxidation of water, Z. Naturforsch. C 32 (1977) 617–626.

[78] C.F. Fowler, Proton evolution from photosystem II stoichiometry and mechanistic considerations, Biochim. Biophys. Acta 462 (1977) 414–421.

[79] F. Rappaport, J. Lavergne, Proton release during successive oxidation steps of the photosynthetic water oxidation process - stoichiometries and pH-dependence, Biochemistry 30 (1991) 10004–10012.

[80] H. Suzuki, M. Sugiura, T. Noguchi, Monitoring proton release during photosynthetic water oxidation in photosystem II by means of isotope-edited infrared spectroscopy, J. Am. Chem. Soc. 131 (2009) 7849–7857.

[81] E. Schlodder, H.T. Witt, Stoichiometry of proton release from the catalytic center in photosynthetic water oxidation, J. Biol. Chem. 274 (1999) 30387–30392.

[82] V. Förster, W. Junge, Stoichiometry and kinetics of proton release upon photosynthetic water oxidation, Photochem. Photobiol. 41 (1985) 183–190.

[83] R. Ahlbrink, M. Haumann, D. Cherepanov, O. Bögershausen, A. Mulkidjanian, W. Junge, Function of Tyrosine Z in water oxidation by Photosystem II: electrostatical promotor instead of hydrogen abstractor, Biochemistry 37 (1998) 1131–1142.

[84] D. Narzi, D. Bovi, L. Guidoni, Pathway for Mn-cluster oxidation by tyrosine-Z in the S_2 state of Photosystem II, Proc. Natl. Acad. Sci. U. S. A. 111 (2014) 8723–8728.

[85] M. Retegan, V. Krewald, F. Mamedov, F. Neese, W. Lubitz, N. Cox, D.A. Pantazis, A five-coordinate Mn(IV) intermediate in biological water oxidation: spectroscopic signature and a pivot mechanism for water binding, Chem. Sci. 7 (2016) 72–84.

[86] K. Yamaguchi, H. Isobe, M. Shoji, S. Yamanaka, M. Okumura, Theory of chemical bonds in metalloenzymes XX: magneto-structural correlations in the $CaMn_4O_5$ cluster in oxygen-evolving complex of photosystem II, Mol. Phys. 114 (2016) 519–546.

[87] K. Cser, I. Vass, Radiative and non-radiative charge recombination pathways in Photosystem II studied by thermoluminescence and chlorophyll fluorescence in the cyanobacterium *Synechocystis* 6803, Biochim. Biophys. Acta 1767 (2007) 233–243.

[88] F. Rappaport, J. Lavergne, Thermoluminescence: theory, Photosynth. Res. 101 (2009) 205–216.

[89] A.W. Rutherford, G. Renger, H. Koike, Y. Inoue, Thermoluminescence as a probe of Photosystem II. The redox and protonation states of the secondary acceptor quinone and the O_2-evolving enzyme, Biochim. Biophys. Acta 767 (1984) 548–556.

[90] Y. Kato, T. Shibamoto, S. Yamamoto, T. Watanabe, N. Ishida, M. Sugiura, F. Rappaport, A. Boussac, Influence of the PsbA1/PsbA3 and Ca^{2+}/Sr^{2+} or Cl^-/Br^- exchanges on the redox potential of the primary quinone Q_A in Photosystem II as revealed by spectro-electrochemistry, Biochim. Biophys. Acta (2012) (1817) 1998–2004.

[91] M. Shoji, H. Isobe, Y. Shigeta, T. Nakajima, K. Yamaguchi, Concerted mechanism of water insertion and O_2 release during the S_4 to S_0 transition of the oxygen-evolving complex in Photosystem II, J. Phys. Chem. B 122 (2018) 6491–6502.

[92] M. Shoji, H. Isobe, S. Yamanaka, Y. Umena, K. Kawakami, N. Kamiya, J.-R. Shen, K. Yamaguchi, Theoretical insight into hydrogen-bonding networks and proton wire for the $CaMn_4O_5$ cluster of photosystem II. Elongation of Mn–Mn distances with hydrogen bonds, Catal. Sci. Technol. 3 (2013) 1831–1848.

[93] P.E.M. Siegbahn, Oxidation by PSII - a quantum chemical approach, in: M. Wikström (Ed.), Mechanisms of Primary Energy Transduction in Biology, The Royal Society of Chemistry, 2017.

[94] I. Zaharieva, H. Dau, M. Haumann, Sequential and coupled proton and electron transfer events in the $S_2 \rightarrow S_3$ transition of photosynthetic water oxidation revealed by time-resolved X-ray absorption spectroscopy, Biochemistry 55 (2016) 6996–7004.

[95] G.T. Babcock, R. Blankenship, K. Sauer, Reaction-kinetics for positive charge accumulation on water side of chloroplast photosystem 2, FEBS Lett. 61 (1976) 286–289.

[96] H. Sakamoto, T. Shimizu, R. Nagao, T. Noguchi, Monitoring the reaction process during the $S_2 \rightarrow S_3$ transition in photosynthetic water oxidation using time-resolved infrared spectroscopy, J. Am. Chem. Soc. 139 (2017) 2022–2029.

[97] A. Klauss, M. Haumann, H. Dau, Seven steps of alternating electron and proton transfer in Photosystem II water oxidation traced by time-resolved photothermal beam deflection at improved sensitivity, J. Phys. Chem. B 119 (2015) 2677–2689.

[98] W. Junge, M. Haumann, R. Ahlbrink, A. Mulkidjanian, J. Clausen, Electrostatics and proton transfer in photosynthetic water oxidation, Philos. Trans. R. Soc. Lond. B 357 (2002) 1407–1418.

[99] M. Haumann, W. Junge, Extent and rate of proton release by photosynthetic water oxidation in thylakoids: electrostatic relaxation versus chemical Production, Biochemistry 33 (1994) 864–872.